

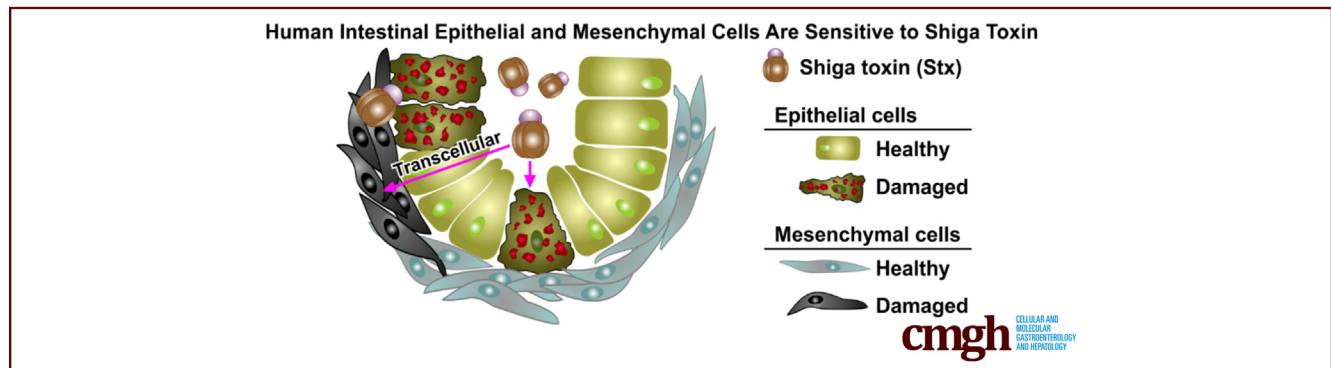
ORIGINAL RESEARCH

Tissue Responses to Shiga Toxin in Human Intestinal Organoids



Suman Pradhan,¹ Sayali S. Karve,¹ Alison A. Weiss,¹ Jennifer Hawkins,² Holly M. Poling,² Michael A. Helmrath,² James M. Wells,³ and Heather A. McCauley³

¹Department of Molecular Genetics, University of Cincinnati, Cincinnati, Ohio; ²Department of Pediatric General and Thoracic Surgery; ³Center for Stem Cell and Organoid Medicine, Division of Developmental Biology, Cincinnati Children's Hospital Medical Center, Cincinnati, Ohio



SUMMARY

Human susceptibility to Shiga toxin is not well modeled in traditional cell culture or experimental animals. Human stem cell–derived intestinal organoids show complex, tissue-level responses to Shiga toxin not previously described, including epithelial mesenchymal cross-talk.

BACKGROUND & AIMS: Shiga toxin (Stx)-producing *Escherichia coli* (eg, O157:H7) infection produces bloody diarrhea, while Stx inhibits protein synthesis and causes the life-threatening systemic complication of hemolytic uremic syndrome. The murine intestinal tract is resistant to O157:H7 and Stx, and human cells in culture fail to model the complex tissue responses to intestinal injury. We used genetically identical, human stem cell–derived intestinal tissues of varying complexity to study Stx toxicity in vitro and in vivo.

METHODS: In vitro susceptibility to apical or basolateral exposure to Stx was assessed using human intestinal organoids (HIOs) derived from embryonic stem cells, or enteroids derived from multipotent intestinal stem cells. HIOs contain a lumen, with a single layer of differentiated epithelium surrounded by mesenchymal cells. Enteroids only contain epithelium. In vivo susceptibility was assessed using HIOs, with or without an enteric nervous system, transplanted into mice.

RESULTS: Stx induced necrosis and apoptotic death in both epithelial and mesenchymal cells. Responses that require protein synthesis (cellular proliferation and wound repair) also were observed. Epithelial barrier function was maintained even after epithelial cell death was seen, and apical to basolateral translocation of Stx was seen. Tissue cross-talk, in which

mesenchymal cell damage caused epithelial cell damage, was observed. Stx induced mesenchymal expression of the epithelial marker E-cadherin, the initial step in mesenchymal–epithelial transition. In vivo responses of HIO transplants injected with Stx mirrored those seen in vitro.

CONCLUSIONS: Intestinal tissue responses to protein synthesis inhibition by Stx are complex. Organoid models allow for an unprecedented examination of human tissue responses to a deadly toxin. (*Cell Mol Gastroenterol Hepatol* 2020;10:171–190; <https://doi.org/10.1016/j.jcmgh.2020.02.006>)

Keywords: Intestinal Tissues; Epithelium; Mesenchyme.

Shiga toxin (Stx) producing *Escherichia coli*, including O157:H7, cause approximately 3 million cases of acute bloody diarrheal disease each year. In addition, approximately 4000 patients develop the life-threatening systemic complication of hemolytic uremic syndrome (HUS),¹ characterized by clot formation, destruction of red blood cells, platelet depletion, and acute kidney failure.² Stx is an AB₅ toxin.^{3,4} The A subunit enzymatically inactivates ribosomes,⁵ halting protein synthesis. The B-pentamer promotes entry of the A subunit into the mammalian cytoplasm. The glycolipid globotriaosylceramide (Gb3) serves as the receptor for Stx,^{6–9} and mice deleted for Gb3 synthase gene (*A4GALT*) are totally resistant to Stx.¹⁰ However, not all cells that express Gb3 are sensitive to Stx, and proper cytoplasmic trafficking to the ribosomes is required for toxin sensitivity.¹¹

Responses to Stx-mediated inhibition of protein synthesis vary by cell type. Cell death can occur by apoptosis or necrosis.^{12–14} The mechanism of cell death can influence

adjacent tissue. Apoptosis does not elicit inflammation when cells are cleared by phagocytosis. However, loss of membrane integrity in necrosis can release toxic cellular contents (eg, lysosomal enzymes) and cause bystander cell damage.^{15,16} Systemic damage can occur in the absence of cellular death (eg, when injured cells release cytokines and chemokines). Platelet activation by Stx-treated endothelial cells triggers the clot formation in the microvasculature that defines HUS.¹⁷

Developing effective interventions for disease resulting from Stx is exacerbated by a lack of tractable model systems. Mice do not develop the symptoms characteristic of HUS, and the murine intestinal tract is resistant to Stx.¹⁸ Advances in stem cell biology have allowed for generation of genetically normal, differentiated human intestinal tissues. Human intestinal organoids (HIOs) are generated by the directed differentiation of pluripotent stem cells.^{19,20} HIOs represent human tissue from the small bowel,¹⁹ the tissues favored for initial attachment of *Escherichia coli* O157:H7.²¹ The HIO epithelium possesses different cell types (enterocytes, Paneth cells, enteroendocrine cells, and goblet cells), and expresses the brush-border marker villin; however deep crypt structures are not seen. The epithelial layer is surrounded by mesenchymal cells with myofibroblast and smooth muscle cell markers.¹⁹ HIOs grown in vitro have a relatively immature tissue structure, however, on transplantation under the mouse kidney capsule HIOs form highly structured villi, proliferating progenitor zones, and crypts.²² In addition, incorporation of enteric neuronal precursors into developing HIOs results in the formation of intestinal tissues with a functional enteric nervous system (ENS) capable of peristalsis.²³ Multipotent intestinal epithelial stem cells obtained from the transplanted HIOs have been used to derive enteroids, which contain differentiated epithelium, but lack mesenchymal cells. We used these human stem cell-derived intestinal tissues to study human intestinal tissue responses to Stx in vivo and in vitro.

Results

HIO Express Gb3, the Stx Receptor

Expression of glycolipid Gb3, the Stx receptor, was assessed. HIO cryosections stained with a monoclonal antibody to Gb3 showed strong staining of the epithelial cells, with weak staining of some mesenchymal cells (Figure 1A). The presence of the transcript for Gb3 synthase (*A4GALT*) also was detected by RNA sequencing (Table 1).

HIOs Are Susceptible to Stx by Luminal or Basolateral Delivery

HIOs are polarized intestinal tissues. Stx introduced into the lumen resembles intestinal exposure to Stx produced by the infecting *E coli*, while addition to the surrounding tissue culture media resembles the interstitial exposure, which would occur after loss of epithelial barrier function or exposure to circulating toxin. To determine whether luminal exposure to Stx disrupts epithelial barrier function, HIOs were microinjected with various doses of Stx in the presence of the fluorescent dye fluorescein isothiocyanate


(FITC). HIO epithelial barrier function was assessed by monitoring retention of fluorescence over time.

Two major forms of Stx include Stx1 and Stx2.²⁴ The Stx2a variant is approximately 100 times more potent than Stx1 in mice,^{25,26} and is expressed more commonly by strains isolated from human disease.^{27–30} Both Stx1 and Stx2a were tested. The distribution and intensity of fluorescence did not change in HIOs injected with saline (Figure 1B–D), suggesting the process of microinjection does not disrupt the integrity of the epithelial barrier. In contrast, significant time- and dose-dependent decreases in fluorescence were observed in HIOs injected with either Stx2a (Figure 1B and C) or Stx1 (Figure 1D), suggesting both forms of Stx mediate leakage from the luminal compartment. We also characterized susceptibility to Stx added to the tissue culture medium, or basolateral exposure, which models interstitial exposure (Figure 1C and D, interstitial). Statistically significant time-dependent decreases in fluorescence were seen for both Stx1 and Stx2a when 30 ng toxin was added to the media, and the magnitude of the response was very similar to 30 ng delivered into the lumen. A total of 10 ng Stx2a and Stx1 microinjected into the lumen caused a statistically significant loss of fluorescence. Because Stx2a is more relevant to human disease, further studies were performed using Stx2a.

Stx2a Treatment Induces Changes in Transcription

RNA sequencing was performed on HIOs at 4 hours (Supplementary Table 1) and at 24 hours (Supplementary Table 2) after injection with phosphate-buffered saline (PBS) (control) or 30 ng Stx2a. HIOs are tissues containing differentiated epithelial cells and mesenchymal cells, and RNA sequencing includes reads from all cells present in the tissues. Even though Stx2a is associated with inhibition of protein synthesis, significant up-regulation in transcription was observed. Setting significance at a *P* value less than .05 and using a 4-fold change compared with the PBS controls as the cut-off level, 4 hours after treatment with Stx2a resulted in 669 differentially expressed genes (414 up-regulated and 255 down-regulated). Of the 18,207 genes identified by RNA sequencing, 15,411 were associated with a Gene Ontology (GO) term. For the up-regulated genes, 347 could be assigned to a GO term. The gene families up-regulated most significantly ($P < 10^{-9}$) by Stx2a were involved primarily in transport (organic hydroxy compound transport [GO:0015850], lipid transport [GO:0006869], and

Abbreviations used in this paper: ENS, enteric nervous system; FITC, fluorescein isothiocyanate; Gb3, globotriaosylceramide; GO, Gene Ontology; HIO, human intestinal organoid; HUS, hemolytic uremic syndrome; IP, intraperitoneal; LPS, lipopolysaccharide; NSG, NOD scid gamma; OGMH, Organoid Growth Media Human; PBS, phosphate-buffered saline; Stx, Shiga toxin; Tcd, *C difficile* toxins; TEER, trans-epithelial electrical resistance.

 Most current article

© 2020 The Authors. Published by Elsevier Inc. on behalf of the AGA Institute. This is an open access article under the CC BY-NC-ND license (<http://creativecommons.org/licenses/by-nc-nd/4.0/>).

2352-345X

<https://doi.org/10.1016/j.jcmgh.2020.02.006>

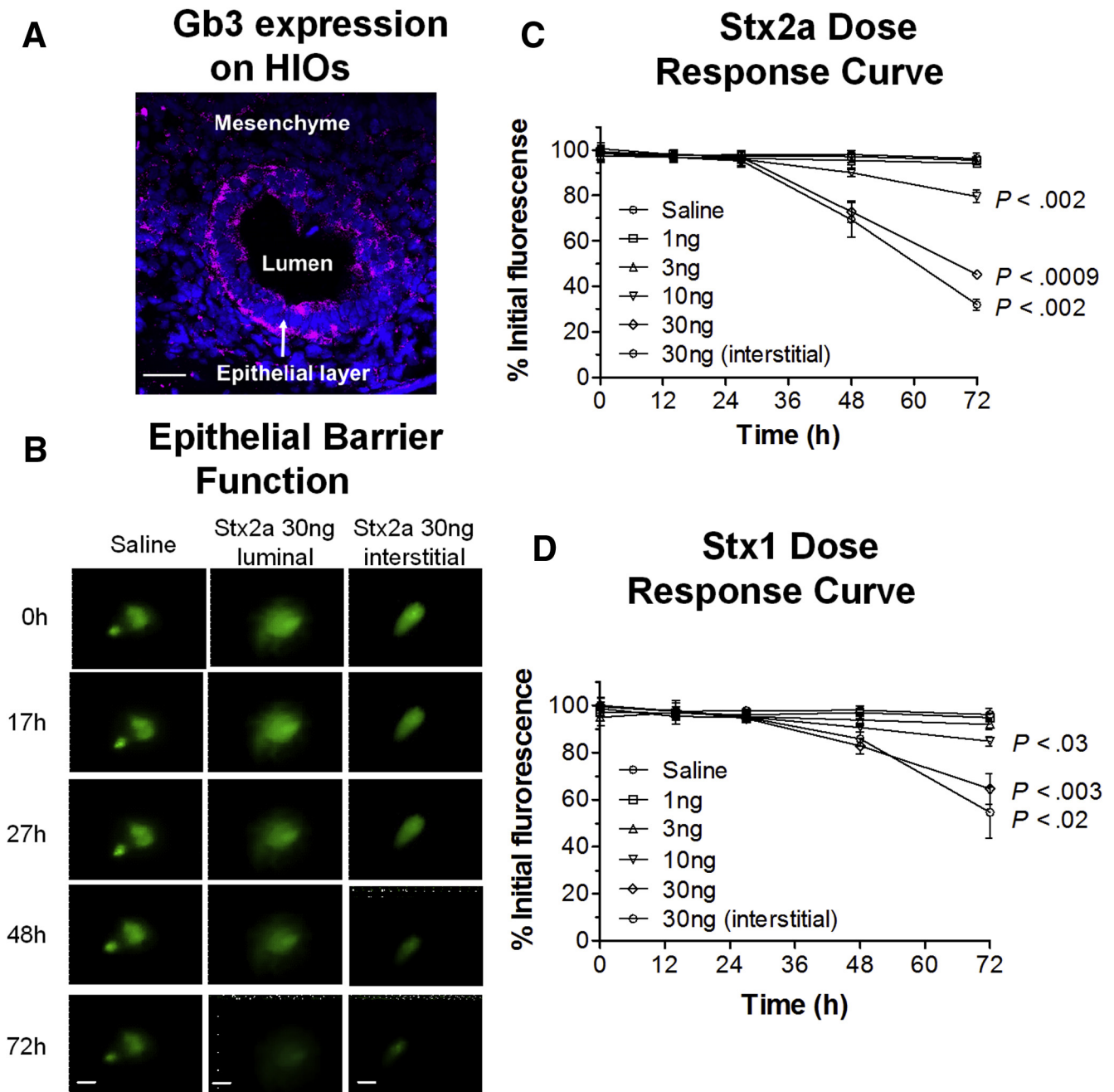


Figure 1. HIOs express the Stx receptor Gb3 and are susceptible to Stx by luminal or basolateral delivery. (A) HIOs express the Stx receptor Gb3. Cryosections were stained for DNA (4',6-diamidino-2-phenylindole, blue), and antibody to Gb3 (red). Intense staining was observed on epithelial cells. Scale bar: 50 μm . (B) Stx causes loss of epithelial barrier function. Representative images of intact HIOs loaded with the fluorescent dye FITC, and exposed to Stx2a (30 ng) introduced by microinjection (luminal exposure) or added to the medium (interstitial exposure) over time. Scale bar: 100 μm . (C and D) Time- and dose-dependent responses to Stx. Toxin was delivered by microinjection (luminal exposure) or added to the medium (interstitial exposure). Epithelial barrier function was assessed by fluorescence retention, quantified by ImageJ, and plotted as the percentage mean at time zero \pm SD, $n = 3$. Values at 72 hours compared with time zero were assessed using 1-way analysis of variance, Dunnett's posttest. (C) HIO sensitivity to Stx2a. (D) HIO sensitivity to Stx1.

anion transport [GO:0006820]), or metabolic processes (lipid metabolic process [GO:0006629], small-molecule metabolic process [GO:0044281], steroid metabolic process [GO:0008202], and organic hydroxy compound metabolic process [GO:1901615]). For down-regulated genes,

216 could be assigned to a GO term. No gene families were down-regulated significantly at $P < 10^{-9}$.

Stx2a expression relative to PBS controls of select intestinal and lineage-specific genes are shown in Table 1. Stx2a caused a statistically significant up-regulation of

Table 1. Stx2a Expression Relative to Controls for Select Intestinal and Lineage-Specific Genes

Symbol	Name	Cellular distribution or function	Stx2a 4 h fold change (<i>P</i> value adjusted) ^a	Stx2a 24 h fold change (<i>P</i> value adjusted) ^a
Epithelial/mesenchymal proteins				
<i>CDH1</i>	Cadherin 1, type 1, E-cadherin	Epithelial Adherens junction	2.4 (.03)	0.94 (.95)
<i>KLF4</i>	Kruppel-like factor 4 (gut)	Transcription factor, up-regulates E-cadherin	5.9 (.00023)	0.86 (.90)
<i>CTNNB1</i>	Catenin β 1 (cadherin-associated protein)	Epithelial Adherens junction	1.1 (.9)	0.96 (.97)
<i>LGALS4</i>	Lectin, galactoside-binding, soluble, 4	Epithelial Adherens junction	17 (6E-08)	0.67 (.68)
<i>TJP2</i>	Tight junction protein 2 (ZO-2)	Epithelial Tight junction	2.0 (.03)	0.91 (.90)
<i>OCLN</i>	Occludin	Epithelial Tight junction	2.4 (.007)	1.2 (.80)
<i>CLDN1</i>	Claudin 1	Epithelial Tight junction	2.8 (.0006)	0.74 (.73)
<i>VIL1</i>	Villin 1	Epithelial Brush border	6.3 (.0005)	0.82 (.80)
<i>ALPI</i>	Alkaline phosphatase, intestinal	Epithelial Enterocytes	55 (.02)	1.3 (.89)
<i>LYZ</i>	Lysozyme	Epithelial Paneth cells	7.3 (.0001)	0.64 (.52)
<i>CHGA</i>	Chromogranin A	Epithelial Enteroendocrine cells	0.99 (1.0)	0.37 (.26)
<i>MUC2</i>	Mucin 2 oligomeric mucus/gel-forming	Epithelial Goblet cells	11 (.0005)	2.7 (.008)
<i>MUC13</i>	Mucin 13, cell surface associated	Epithelial Mucus	10 (8E-06)	0.94 (.98)
<i>MUC17</i>	Mucin 17, cell surface associated	Epithelial Mucus	14 (.001)	3.1 (.97)
<i>TFF1</i>	Trefoil factor 1	Epithelial Mucosal layer	32 (3E-11)	1.4 (.80)
<i>TFF2</i>	Trefoil factor 2	Epithelial Mucosal layer	58 (4E-10)	2.0 (.60)
<i>TFF3</i>	Trefoil factor 3 (intestinal)	Epithelial Mucosal layer	15 (5E-07)	1.3 (.83)
<i>VIM</i>	Vimentin	Mucosal layer Mesenchyme	0.89 (.8)	0.92 (.93)
Immune response				
<i>IL18</i>	Interleukin 18	Immune response	12 (6E-08)	0.40 (.41)
<i>CCL15</i>	Chemokine (C-C motif) ligand 15	Immune response	32 (1E-08)	0.9 (.95)
Shiga toxin receptor, proliferation, apoptosis				
<i>A4GALT</i>	Gb3 synthase	Shiga toxin receptor	0.10 (.3)	1.9 (.86)
<i>EGFR</i>	Epidermal growth factor receptor	Cellular growth	0.37 (9E-06)	2.1 (.02)
<i>MKI67</i>	Marker of proliferation Ki-67	Cellular growth	0.30 (2E-08)	1.7 (.50)
<i>XBP1</i>	X-box binding protein 1	ER stress	1.5 (.19)	0.69 (.53)
<i>DNAJB9</i>	DnaJ (Hsp40) homolog, subfamily B, member 9	ER stress	1.3 (.53)	1.1 (.97)
<i>DDIT3</i>	CHOP, DNA-damage-inducible transcript 3	ER stress	1.5 (.60)	1.1 (.94)
<i>BCL2</i>	B-cell CLL/lymphoma 2	Anti-apoptotic	0.32 (.17)	0.69 (.79)
<i>TNFRSF10B</i>	DR5, tumor necrosis factor receptor superfamily, member 10b	Pro-apoptotic	0.97 (.96)	0.89 (.88)
<i>NLRP3</i>	NLR family, CARD domain-containing 4	Interacts with the apoptosis-associated speck-like protein PYCARD	0.55 (.88)	0.52 (.76)
<i>PYCARD</i>	PYD and CARD domain containing	Promotes caspase-mediated apoptosis	2.2 (.43)	0.61 (.68)
<i>CSP4</i>	Caspase-4	Inflammatory caspase, promotes pyroptosis through gasdermin D cleavage	2.3 (.04)	0.83 (.87)

ER, endoplasmic reticulum.

^aAdjusted for false-discovery rate.

epithelial structural proteins (adherens junction proteins and tight junction proteins), and lineage-specific proteins (epithelial brush-border villin 1, enterocyte intestinal alkaline phosphatase, Paneth cell lysozyme, and goblet cell MUC2). Other up-regulated factors include mucins (MUC13 and MUC17) and trefoil factors (TFF1, TFF2, and TFF3), which are involved in forming and stabilizing the mucus layer. Two cytokine factors, interleukin 18 and CCL15, were up-regulated significantly. RNA sequencing performed at 24 hours after Stx2a injection showed few differentially regulated genes (Supplementary Table 2). Compared with control, only 25 genes were up-regulated significantly ($P < .05$) 4-fold or more, and 25 were down-regulated significantly.

Stx2a Induces Cellular Death and Proliferation

Transcription of both epidermal growth factor receptor and a marker of proliferation, Ki-67, were down-regulated significantly compared with PBS controls at 4 hours after injection of Stx2a (Table 1). However, 24 hours after injection, both were up-regulated, with epidermal growth factor receptor expression reaching significance. To determine if there was a population of proliferating cells, we stained HIOs with Ki-67 to assess proliferation and Sytox-green (Invitrogen, Waltham, MA) to assess cellular necrosis. Sytox-green is a membrane-impermeable DNA dye. Staining with Sytox-green indicates loss of membrane integrity, consistent with cellular necrosis. Control HIOs appeared to be quiescent; a few proliferating Ki-67-positive cells (Figure 2A, red) were seen distributed in both the epithelial and mesenchymal layers. Very few necrotic cells were visible (Figure 2A, green). In the Stx2a-treated HIOs, separate clusters of numerous necrotic (green-stained cells) and proliferating (red-stained cells) were observed. Cellular staining for proliferating cells and necrotic cells was quantified. Stx2a treatment from either surface resulted in significantly increased staining for cellular necrosis (Figure 2B) and proliferation (Figure 2C). Although cellular death resulting from Stx2a was anticipated, cellular proliferation was unexpected, and likely represents an adaptive response to repair tissue damage. Necrotic responses were similar regardless of whether Stx2a was injected into the lumen or introduced into the medium (interstitial); however, more proliferation was seen with interstitial exposure.

Time-Dependent Responses to Stx2a

We imaged HIOs engineered to express mRuby2 under control of the E-cadherin gene (CDH1-mRuby2) in the presence of SYTOX green up to 148 hours after exposure to evaluate cellular death (Figure 2D). In control HIOs, the diffuse mesenchymal layer is distinct from the compact epithelial layer where mRuby2 E-cadherin is expressed (Figure 2D, control). E-cadherin expression increased with time in untreated control HIOs (Figure 2D and E). In the Stx2a-treated HIOs, mRuby2 E-cadherin expression increased for up to 72 hours, then decreased, and E-cadherin fluorescence accumulated in the lumen, likely owing

to extrusion of dead epithelial cells. Very little cell death, as evidenced by green-stained cells, was noted in the absence of Stx2a, whereas necrosis increased with time in the Stx2a-treated HIOs (Figure 2D and F).

Stx2a Induces Apoptosis and Necrosis in Mesenchymal Cells

To assess mesenchymal responses in the absence of the epithelium, mesenchyme from the CDH1-mRuby2 HIOs was separated mechanically from the epithelial layer. Treatment with Stx2a resulted in a statistically significant increase in apoptosis, as evidenced by staining for activated caspase 3 (Figure 3A and B). As seen in Figure 2D, mesenchymal cells treated with Stx2a were stained with Sytox Green (Figure 3C), and pretreatment with Necrox-5 before addition of Stx2a greatly reduced necrosis (Figure 3D). Necrox-5 (Enzo Life Sciences, Inc, Farmingdale, NY) is a cell-permeable inhibitor of necrosis. It acts by localizing in the mitochondria and blocking oxidative stress-induced cell death. Similarly, co-injection of HIOs with Necrox-5 with Stx2a significantly reduced necrosis in both mesenchymal and epithelial cells (Figure 4).

Stx2a Induces E-cadherin Expression in Mesenchymal Cells

In HIOs, the mesenchymal region, as evidenced by staining with vimentin, is completely distinct from the epithelium, which stains with E-cadherin. In Stx2a-treated HIOs, in some areas the cells expressed only 1 marker, however, in other areas the cells were stained for both vimentin and E-cadherin (Figure 5A, circle), as evidenced by the yellow signal in the co-stained images. Similarly, serial sections stained for the individual markers also showed staining for both markers.

Co-expression of 2 different lineage-specific markers is consistent with mesenchymal-epithelial transition, a response to wounding in which mesenchymal cells convert to epithelial cells. Evidence for mesenchymal-epithelial transition also was seen in purified mesenchymal cells. In untreated mesenchymal cells, expression of vimentin was detected, while expression of E-cadherin protein or mRuby2 from the E-cadherin fusion was not detected (Figure 5B-D). In contrast, after Stx2a treatment, the purified mesenchymal cells showed a statistically significant increased expression of mRuby2 reporter and staining with antibody to E-cadherin (Figure 5B-D). Regulation of E-cadherin transcription by the transcription factor Kruppel-like factor 4 plays a key role in interconversion of epithelial and mesenchymal cells.³¹ RNA sequencing (Table 1) showed that Stx2a up-regulated expression of E-cadherin and Kruppel-like factor 4.

Mesenchymal-Epithelial Transition Is a Generalized Response to Intestinal Tissue Damage by Bacterial Toxins

Purified mesenchymal cells were treated with different bacterial toxins, including microcystin-LR, which inactivates protein phosphatases, *Clostridioides difficile* toxins A and B

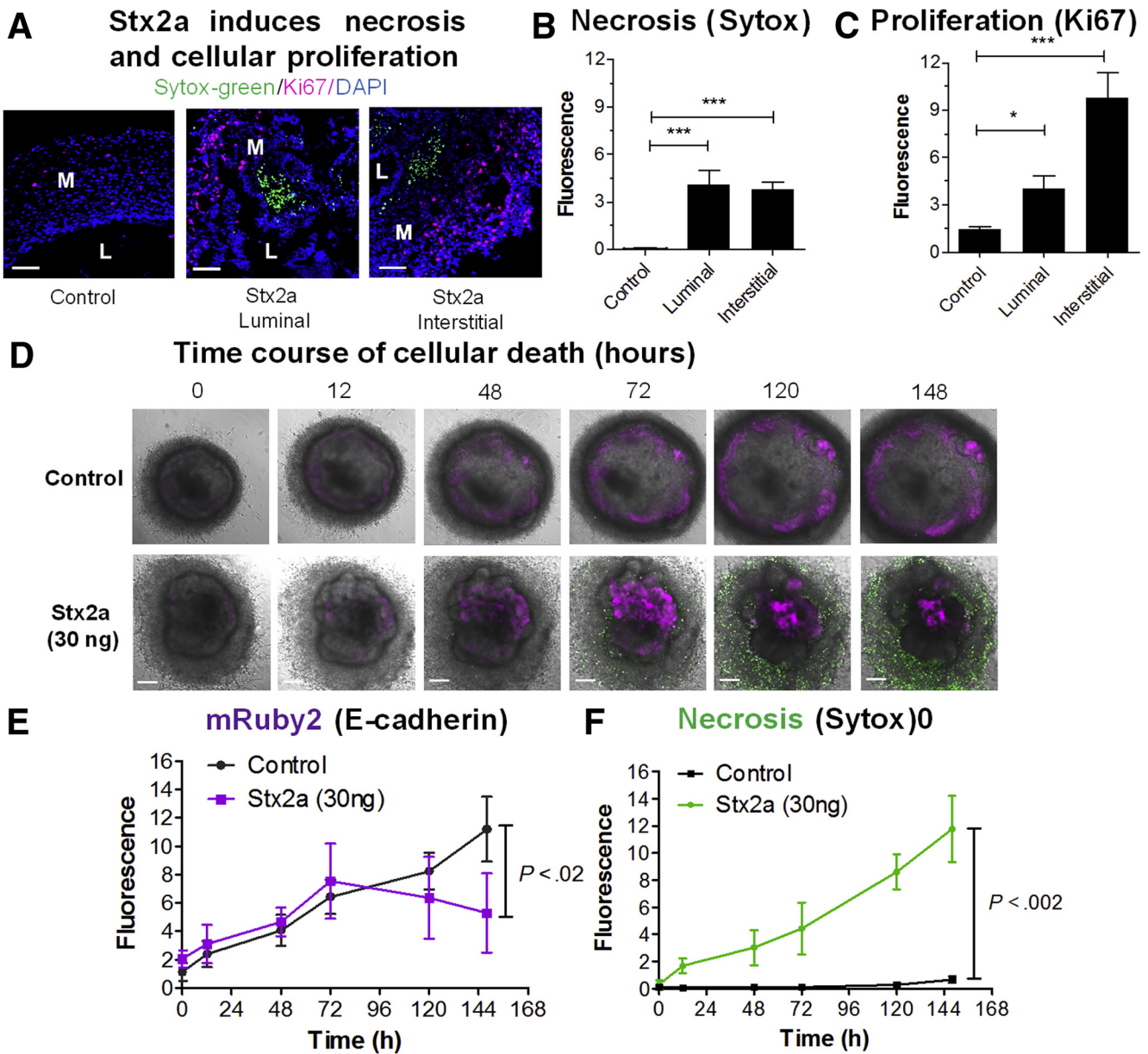


Figure 2. Epithelial and mesenchymal cells are sensitive to Stx2a. (A) Stx2a induces necrosis and cellular proliferation. HIOs were incubated for 27 hours with Stx2a (30 ng) by microinjection (luminal exposure) or addition to the medium (interstitial exposure). Cryosections were stained for necrosis (Sytox-green), proliferation (Ki-67, red), and DNA (4',6-diamidino-2-phenylindole [DAPI], blue). Scale bar: 50 μ m. (B and C) Fluorescence intensity was quantified using ImageJ software and plotted as means \pm SD, n = 3. Statistical significance compared with saline control was assessed using 1-way analysis of variance, Dunnett's posttest. * P = .01 to .05; *** P < .001. (B) Cellular death by necrosis (Sytox-green fluorescence). (C) Cellular proliferation (Ki-67 fluorescence). (D) Time course of cellular death. Serial images of intact HIOs with mRuby2 fused to the promoter of E-cadherin grown in the presence of 5 μ mol/L Sytox-green. Saline (control, top) or 30 ng Stx2a (bottom) were added to the medium at time zero and imaged at the indicated times (hours). Representative images of experiments performed in triplicate. Scale bar: 100 μ m. (E and F) Fluorescence intensity quantified using ImageJ software, plotted as means \pm SD, n = 3. Statistical significance at 148 hours compared with saline control was assessed using a 2-tailed, unpaired t test. (E) Stx2a causes loss of mRuby2 (E-cadherin expression). (F) Stx2a causes necrosis (Sytox-green). L, lumen; M, mesenchyme.

(TcdA and TcdB), which inactivate small guanosine triphosphatases, and bacterial lipopolysaccharide (LPS). E-cadherin (m-Ruby) expression was induced in mesenchymal cells treated with the bacterial toxins, but not LPS (Figure 6).

Stx2a Induces Necrosis and Apoptosis in Epithelial Cells

Enteroids, propagated from differentiated multipotent epithelial stem cells, possess different epithelial cell lineages, but unlike HIOs they lack mesenchymal cells. An

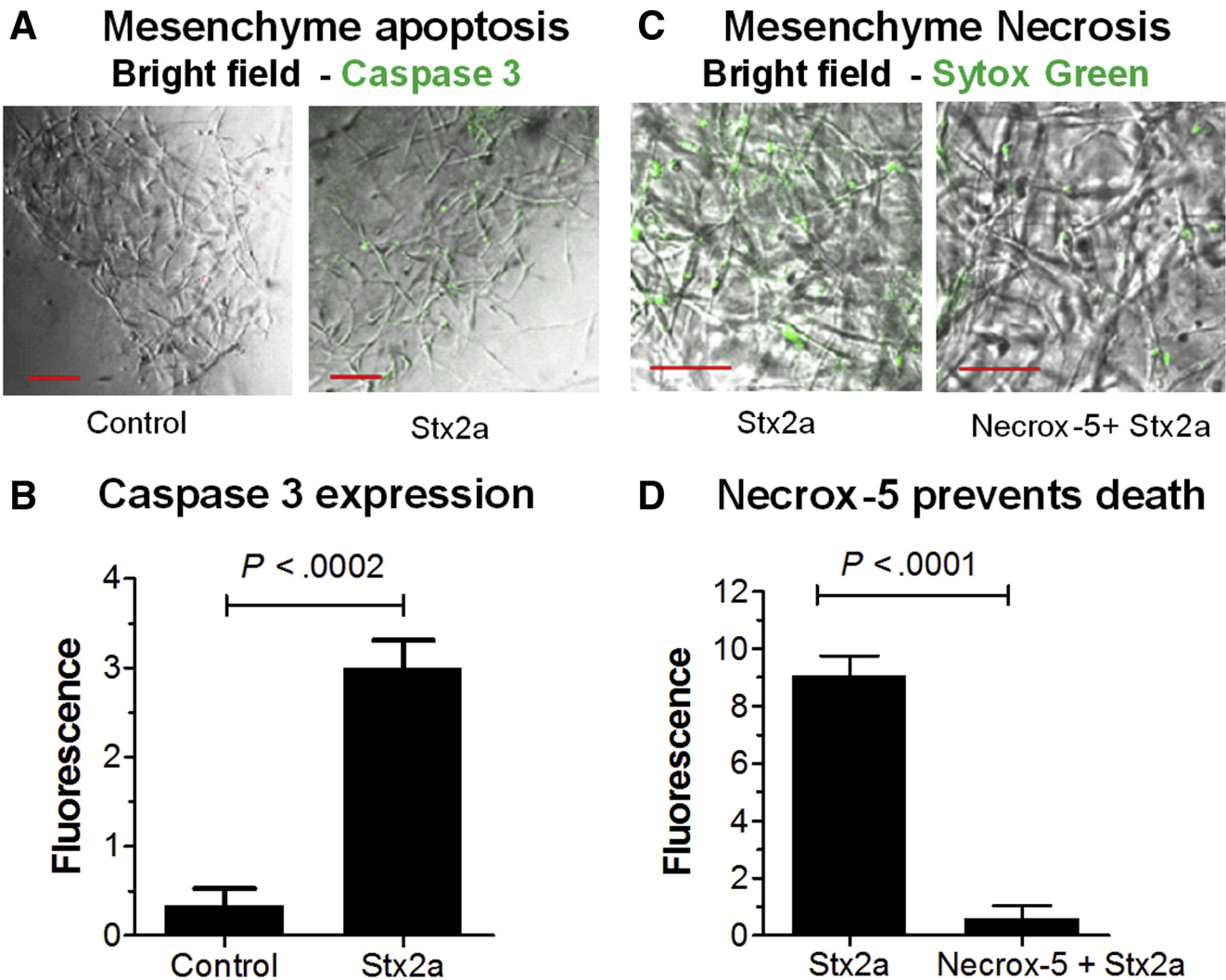


Figure 3. Stx2a induces apoptosis and necrosis in isolated mesenchymal cells. (A) Stx2a induces apoptosis in isolated mesenchymal cells. Mesenchymal cells derived from mRuby2 E-cadherin HIOs challenged by addition of Stx2a (30 ng) were incubated for 27 hours. Cells were stained for apoptosis (Caspase 3). Scale bar: 100 μm . (B) Caspase 3 quantification. Fluorescence intensity was quantified using ImageJ software and plotted as means \pm SD, $n = 3$. Statistical significance was assessed using a 2-tailed, unpaired t test. (C) Stx2a induces necrosis in isolated mesenchymal cells. Mesenchymal cells derived from mRuby2 E-cadherin HIOs were pretreated with or without 2 $\mu\text{mol/L}$ antinecrotic factor Necrox-5 for 1 hour before addition of Stx2a (30 ng). The cells were incubated for 27 hours and stained for Sytox-green. Scale bar: 50 μm . Representative images of experiments performed in triplicate. (D) Sytox-green quantification. Fluorescence intensity was quantified using ImageJ software and plotted as means \pm SD, $n = 3$. Statistical significance was assessed using a 2-tailed, unpaired t test.

enteroid line developed from the H1 HIO line after transplantation into a mouse was used to examine responses to Stx2a in the absence of mesenchymal cells. Stx2a was introduced into the enteroids by microinjection (luminal exposure) or added to the media (interstitial exposure), followed by staining with Sytox to assess necrosis, and activated caspase 3 to assess apoptosis (Figure 7). Both necrosis and apoptosis were observed (Figure 7B and C). Interestingly, in contrast to the HIOs, which were susceptible to Stx2a via luminal or interstitial exposure (Figures 1 and 2) at 27 hours after microinjection, enteroid cell death was seen only when Stx2a was injected into the lumen.

Epithelial Cells Transport Stx From the Lumen to the Basolateral Surface

Mesenchymal necrosis (Figure 2A) was seen in HIOs microinjected with Stx before the epithelial barrier function was lost (Figure 1C), suggesting luminal toxin can access the mesenchymal cells. Previous studies using the human small intestinal cell line Caco-2 showed that Stx can cross the epithelial barrier by intracellular transcytosis.³² To determine if transcytosis was occurring in the human epithelial tissues, enteroids were grown as 2-dimensional monolayers in Transwells. Establishment of epithelial barrier function (Figure 8A) was assessed by monitoring transepithelial electrical resistance (TEER). After 25 days, when the TEER

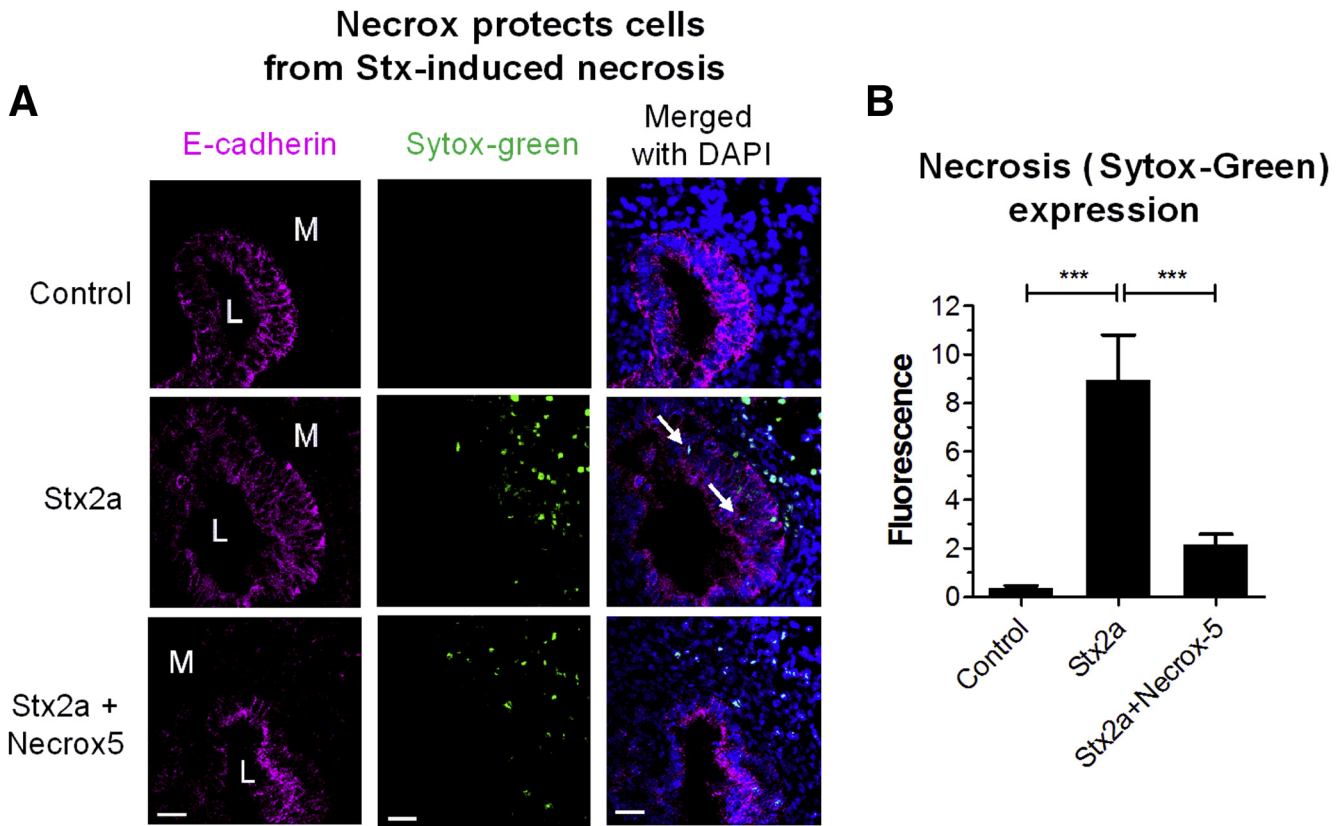


Figure 4. Necrox protects HIOs from Stx-induced necrosis. (A) HIOs were microinjected with Stx2a (30 ng) and Necrox 5 (2 μ mol/L) and incubated for 27 hours. Cryosections were stained for necrosis (Sytox-Green). Scale bar: 100 μ m. Representative images of experiments performed in triplicate are shown. (B) Cellular death by necrosis was quantified by fluorescence using ImageJ software, and plotted as means \pm SD, n = 3. Statistical significance compared with saline control was assessed using 1-way analysis of variance, Bonferroni posttest; *** P < .0001. DAPI, 4',6-diamidino-2-phenylindole; L, lumen; M, mesenchyme.

plateaued, the monolayer was challenged by addition of 30 ng Stx2a to the upper chamber, corresponding to luminal exposure. Barrier function was verified by adding FITC-dextran to the upper chamber 24 hours before adding Stx2a (Figure 8B). After 48 hours, FITC fluorescence was detected in the lower chamber in wells lacking epithelial cells, but not in wells with the untreated or Stx2a-treated monolayers. TEER remained fairly constant in both control and Stx2a-treated monolayers for an additional 15 days (Figure 8A), showing that the epithelial barrier remained intact. However, starting at day 37 and going to day 40, the Stx2a-treated monolayers showed a small but statistically significant (P < .04 to .009) loss of TEER compared with the untreated control monolayers. At day 40, the monolayers were examined by confocal microscopy. Differences were observed between the control and Stx2a-treated monolayers. The Stx2a-treated monolayers showed significantly more cell death (Sytox staining) compared with the control (Figure 9A–C). In addition, the Stx2a-treated monolayer had significantly reduced levels of polymerized actin (Figure 9D–F).

To assess transcytosis (Figure 8C), the culture media from the lower chamber was recovered 24 hours after Stx2a was added to the luminal side. Toxin activity was assessed by adding the medium to cultures of purified mesenchymal cells (Figure 8D). Addition of media from the Stx2a-treated cultures

resulted in significantly increased staining with Sytox-green, indicating necrotic cell death (Figure 8D). To determine whether cell death was caused by Stx2a, neutralizing monoclonal antibodies to the Stx2a A and B subunits were added to the media. Sytox staining was decreased significantly in the presence of neutralizing antibody (Figure 8D), suggesting the necrotic response was caused by Stx2a, which was transferred from the apical to the basolateral surface in the absence of loss of epithelial barrier function.

In Vivo Susceptibility to Stx2a Using Human Organoids Transplanted Into Mice

Human intestinal organoids implanted under the kidney capsule of immunodeficient NOD scid gamma (NSG) mice become vascularized, grow, and acquire a more mature intestinal phenotype than HIOs grown in vitro.²² Furthermore, HIOs integrated with stem cells differentiated along the neuronal pathway can form intestinal tissue with an ENS, and these HIO + ENS tissues show peristalsis.²³

Susceptibility of Mice to Stx2a Is Dependent on Mode of Delivery

To determine whether HIO and HIO + ENS organoids transplanted into mice could serve as an in vivo

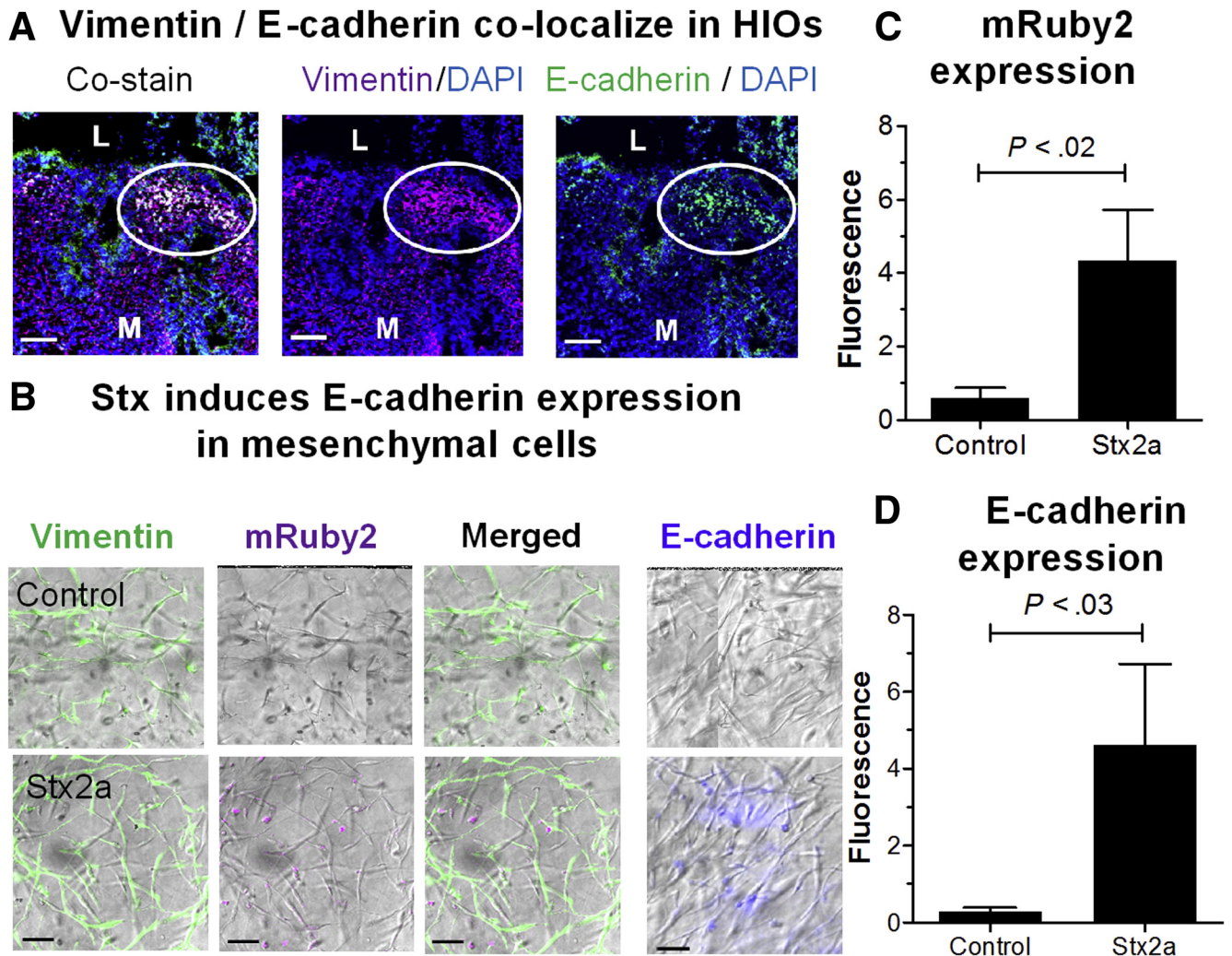


Figure 5. Stx2a induces E-cadherin expression in mesenchymal cells. (A) Cellular co-localization of vimentin and E-cadherin. HIOs were incubated for 27 hours with Stx2a. Serial cryosections were co-stained for DNA (4',6-diamidino-2-phenylindole [DAPI], blue), vimentin (red) to identify mesenchymal cells, and E-cadherin (green) to detect epithelial cells (left, co-stained) or stained for DNA and vimentin (center), or DNA and E-cadherin (right). White circles indicate the region where cells were stained with both markers. Scale bar: 50 μ m. Representative images of experiments performed in triplicate. (B) Isolated mesenchymal cells derived from mRuby2 E-cadherin HIOs were treated with Stx2a (30 ng) in 500 μ L medium for 27 hours, and stained for vimentin (green), E-cadherin (blue), or mRuby2 (red). Representative bright-field images merged with indicated fluorescent stains of experiments performed in triplicate. Scale bar: 50 μ m. (C and D). Fluorescence intensity at 27 hours was quantified using ImageJ software, and plotted as means \pm SD, $n = 3$. Statistical significance was assessed using a 2-tailed, unpaired t test. (C) Quantification of mRuby2 expression in isolated mesenchymal cells. L, lumen; M, mesenchyme.

system to study the human intestinal responses to Stx, we first assessed the susceptibility of NSG mice to Stx. Outbred mice are extremely sensitive to Stx2a delivered systemically by intraperitoneal (IP) injection,⁴ and 10 ng typically is lethal; however, they are highly resistant to Stx2a delivered orally by gavage.¹⁸ To determine if this also is true for the immunodeficient NSG mice, mice were challenged by IP injection or gavage with Stx2a at 10 ng, 100 ng, or 1000 ng (Figure 10A). Consistent with immunocompetent mice, all NSG mice receiving 100 or 1000 ng of Stx2a systemically by IP injection died, and 1 of 4 mice receiving 10 ng died. In contrast, NSG mice were highly resistant to oral

delivery of Stx2a by gavage, only 1 mouse challenged at the highest dose (1000 ng) died.

Injection of Stx2a Into Transplanted Human Organoids Caused Weight Loss in Mice

To investigate in vivo susceptibility to Stx2a, HIO and HIO + ENS organoids were transplanted under the mouse kidney capsule and allowed to mature for 2 months. PBS or Stx2a was injected into the graft and the mice were weighed daily. Mice injected with PBS appeared healthy and did not show weight loss (Figure 10B and C). Mice injected with 1 ng Stx2a also appeared healthy (data not shown). Injection of 10 ng Stx2a caused statistically significant weight loss when

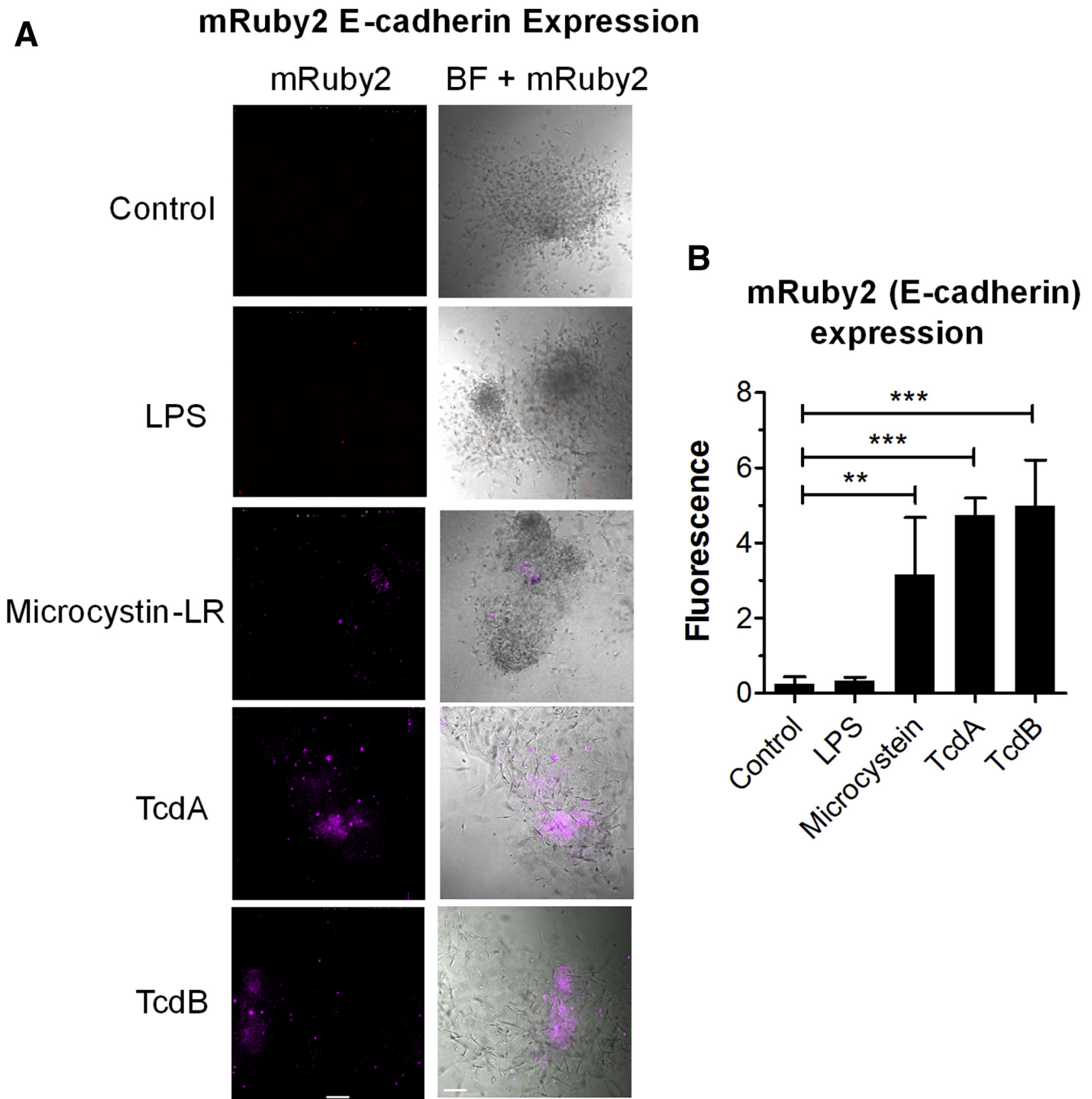


Figure 6. Mesenchymal–epithelial transition is induced by other bacterial toxins. (A) Isolated mesenchymal cells derived from mRuby2 E-cadherin HIOs were challenged by addition of LPS (10 ng), microcystin-LR (10 ng), TcdA (100 ng), or TcdB (100 ng) in 500 μ L gut media. Scale bar: 100 μ m. Left: fluorescent (mRuby2) image shown alone. Right: merged with bright-field (BF) image. Representative images of experiments performed in triplicate are shown. (B) Quantification of E-cadherin–mRuby2 expression in isolated mesenchymal cells. Fluorescence intensity at 72 hours after exposure was quantified by ImageJ software, and plotted as means \pm SD, $n = 3$. Statistical significance was assessed using 1-way analysis of variance, Dunnett's posttest; ** $P = .001$ to $.01$; *** $P = .0001$.

injected into the HIO and HIO + ENS transplants. Some, but not all, animals showed symptoms of disease, including huddling in the corner, slow movements, hunched, heavy breathing, lethargy, or loss of body hair (Table 2). Mice with HIO + ENS transplants appeared to be more susceptible to Stx2a than mice with HIO transplants, and were studied in greater detail.

In Vivo Exposure to Stx2a-Damaged Organoid Transplants

Mice were killed 4 days after injection, kidneys were harvested, and then examined histologically. As reported previously, a mature intestinal phenotype with well-developed crypts was seen in the PBS-injected mice

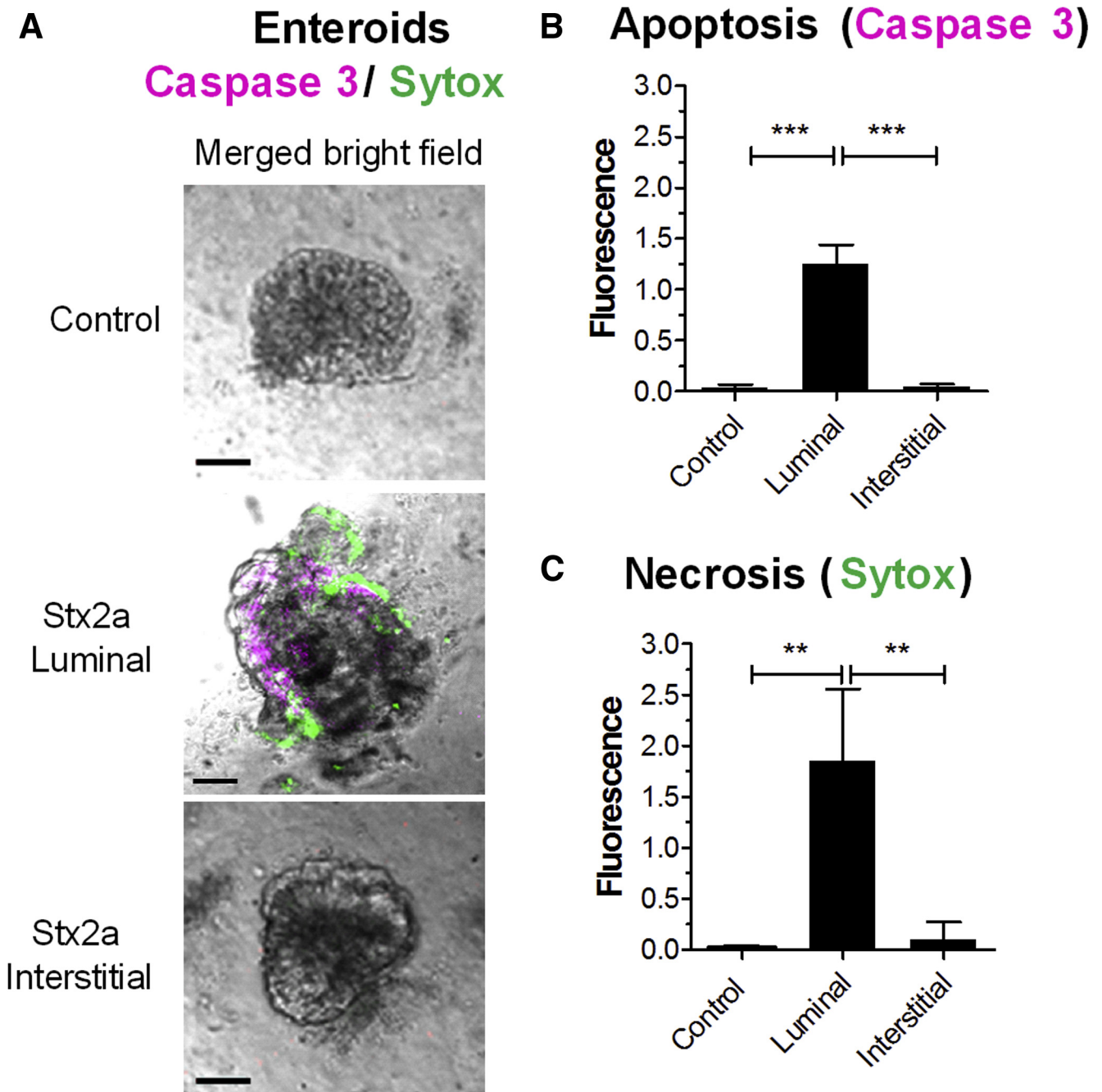


Figure 7. Stx2a induces necrosis and apoptosis in epithelial cells. (A) Enteroids derived from a transplanted HIO were challenged with Stx2a by luminal or interstitial exposure, stained for necrosis (Sytox-green), and whole-mount tissues were stained for apoptosis (caspase 3, red). Scale bar: 100 μ m. Representative images of experiments performed in triplicate. (B and C) Cellular death quantified by fluorescence using ImageJ software, and plotted as means \pm SD, $n = 3$. Statistical significance compared with saline control was assessed using 1-way analysis of variance, Bonferroni posttest; ** $P = .001$ to $.01$; *** $P < .0001$. (B) Death by apoptosis (caspase 3). (C) Death by necrosis (Sytox).

(Figure 10D). For HIO + ENS injected with Stx2a, moderate to significant blood accumulation was seen in the villi and mesenchyme of the transplants (Figure 10E), and epithelial damage was observed in all 3 mice (Table 2). The mouse kidney tissue appeared to be healthy, although regions of fibrosis were seen in both control and Stx-

treated kidneys, likely resulting from healing after the initial implantation surgery.

Stx2a Induces Apoptosis In Vivo

Induction of apoptosis was assessed by staining for activated caspase 3 and co-staining with E-cadherin.

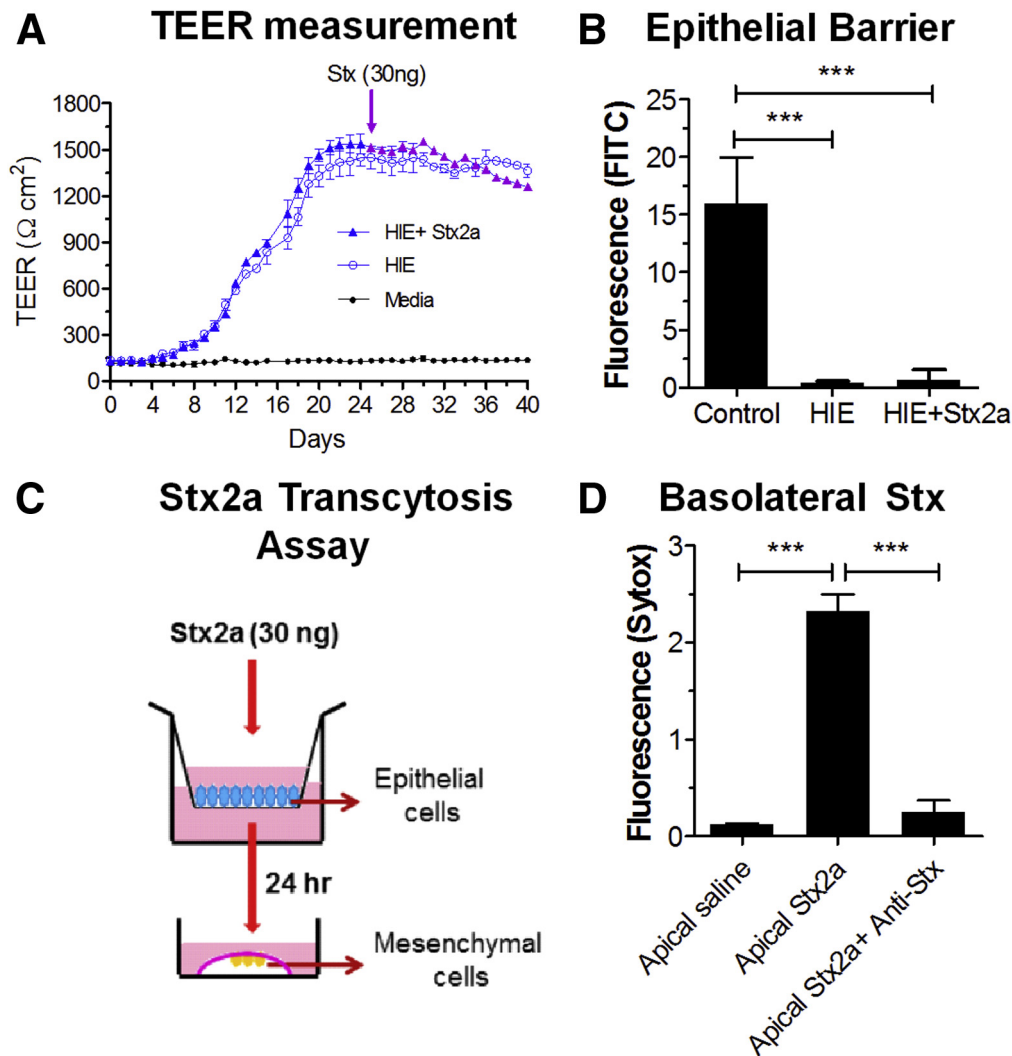


Figure 8. Epithelial cells transport Stx from the lumen to the basolateral surface. (A) TEER measurements in enteroid monolayers formed in Transwells. Stx2a (30 ng) was added to the apical media (upper chamber) of the Transwell on day 25. Means \pm SD of experiments performed in triplicate is plotted. (B) Epithelial barrier function was verified. FITC-dextran (0.5 μ mol/L) was added to the upper chamber on day 24 and Stx2a (30 ng) was added on day 25. Fluorescence in the lower chamber was assessed 24 hours later (day 26). Fluorescence was quantified using ImageJ software, and plotted as means \pm SD. Statistical significance compared with saline control was assessed using 1-way analysis of variance, Dunnett's posttest. $***P < .0001$, $n = 3$. (C) Schematic representation of the Stx2a toxicity assay to detect transcytosis. Stx2a (30 ng) was added to the luminal side of the enteroid monolayer (upper chamber) on day 25. The basolateral medium was isolated from the lower chamber 24 hours later and added to mRuby2-expressing mesenchymal cells isolated from HIOs. (D) Stx2a added to the apical surface was recovered in the basolateral medium. Mesenchymal cells were incubated for 27 hours with basolateral medium (lower chamber) from the Stx2a-treated epithelial monolayers and stained with Sytox green, with or without neutralizing monoclonal antibodies to the Stx2a A and B subunits. Statistical significance compared with saline control was assessed using 1-way analysis of variance, Bonferroni multiple comparison posttest. $***P < 0.0001$, $n = 3$.

Little caspase 3 staining was seen in the control, PBS-injected HIO + ENS (Figure 10F). In contrast, extensive caspase 3 staining was seen in the HIO + ENS challenged with Stx2a, and this difference was statistically significant (Figure 10G). The method for harvesting and fixing the kidneys damages cell permeability, and it was not possible to assess cellular necrosis using the SYTOX stain.

HIO + ENS Transplants Show Evidence of Co-expression of E-Cadherin and Vimentin

Cryosections of the transplanted organoids were costained for the epithelial marker E-cadherin, and the mesenchymal marker vimentin. In control HIO + ENS, deep crypt structures were seen, bordered by green-staining epithelial cells expressing E-cadherin, with red vimentin-stained areas in the interior of the crypt (Figure 10H,

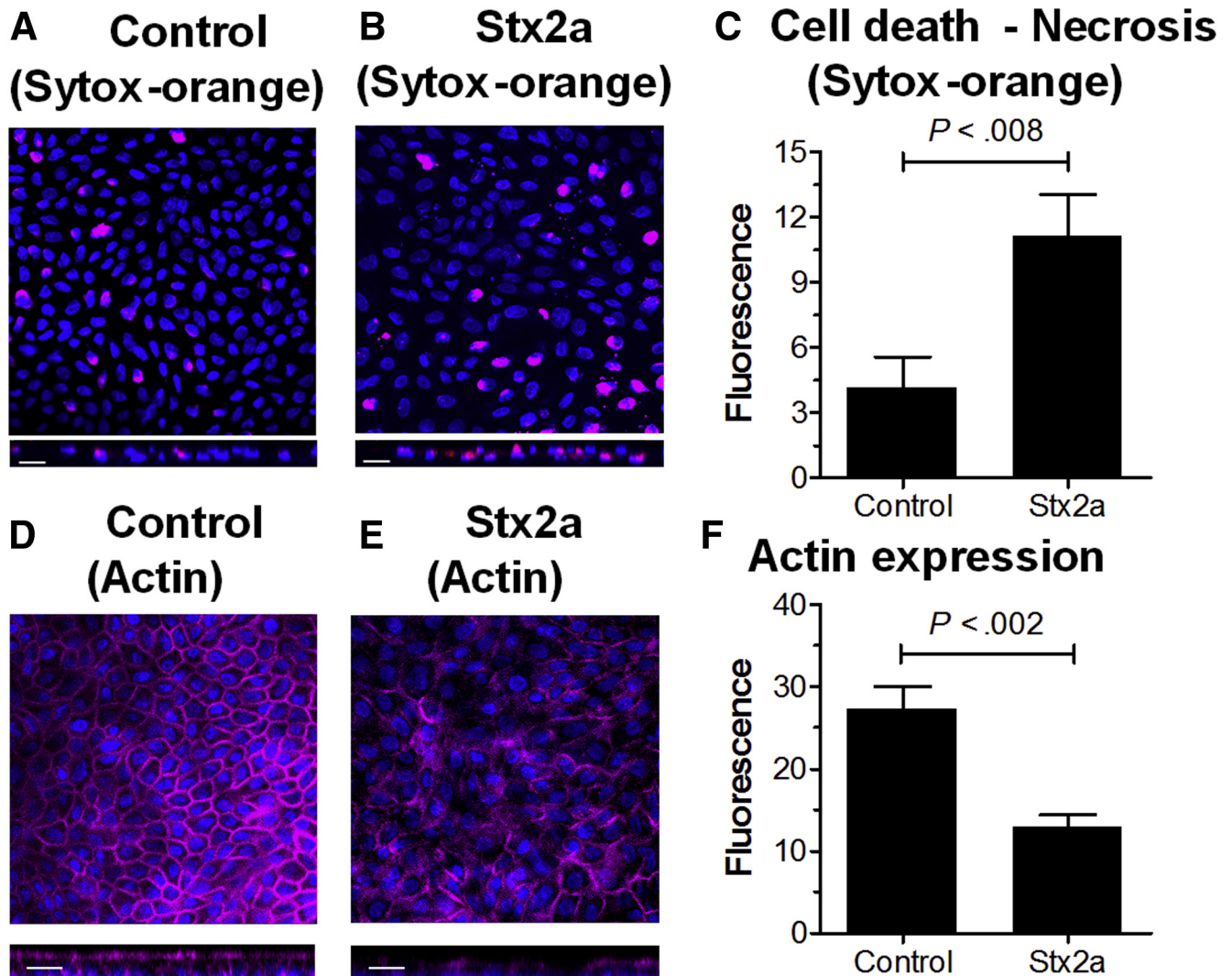


Figure 9. Microscopic characterization of Stx2a-treated monolayers. (A and B) Stx2a induces necrosis. Day 40 HIE monolayers from Figure 8 were stained for necrosis (SYTOX-orange) and DNA (4',6-diamidino-2-phenylindole, blue). *Top*: Confocal X-Y images are shown. *Bottom*: Z-stack is shown. Representative images of experiments performed in triplicate are shown. Scale bar: 20 μ m. (A) Control monolayer. (B) Stx2a-treated monolayer. (C) Stx causes necrosis. Fluorescence intensity was quantified using ImageJ software and plotted as means \pm SD, $n = 3$. Statistical significance compared with saline control was assessed using a 2-tailed, unpaired t test. (D and E) Stx2a disrupts actin expression. Day 40 HIE monolayers from Figure 8 were fixed and stained for polymerized actin (phalloidin, red) and DNA (4',6-diamidino-2-phenylindole, blue). *Top*: Confocal X-Y images are shown. *Bottom*: Z-stack is shown. Representative images of experiments performed in triplicate are shown. Scale bar: 20 μ m. (D) Control monolayer. (E) Stx2a-treated monolayer. (F) Stx alters actin expression. Fluorescence intensity was quantified using ImageJ software and plotted as means \pm SD, $n = 3$. Statistical significance compared with saline control was assessed using a 2-tailed, unpaired t test.

control). In contrast, in HIO + ENS tissues challenged with Stx2a, significant yellow-stained regions, corresponding to co-staining with E-cadherin and vimentin, were seen (Figure 10H, Stx2a), similar to the co-expression of E-cadherin and vimentin seen in Figure 5, suggesting that cellular transition, perhaps mesenchymal-epithelial transition, was occurring in vivo as well as in vitro.

Discussion

Reports regarding expression of glycolipid Gb3, the Stx receptor, on human intestine have been inconsistent. For

negative reports, the inability to detect Gb3 could be owing to technical limitations. Zumbun et al³³ showed specific binding of Stx1 and Stx2 toxin to human colonic epithelial cells, and detected transcripts for Gb3 synthase. Sensitivity to Stx2a has been observed in human intestinal explants treated with Stx2a, suggesting they must express the receptor.³⁴ By using HIOs, we showed staining with antibody to Gb3, the presence of the Gb3 synthase transcript, and, more importantly, susceptibility of epithelial and mesenchymal cells to Stx.

In this study, we examined genetically identical human intestinal tissues of varying complexity, both in vitro and in vivo, and uncovered intimate communication between the

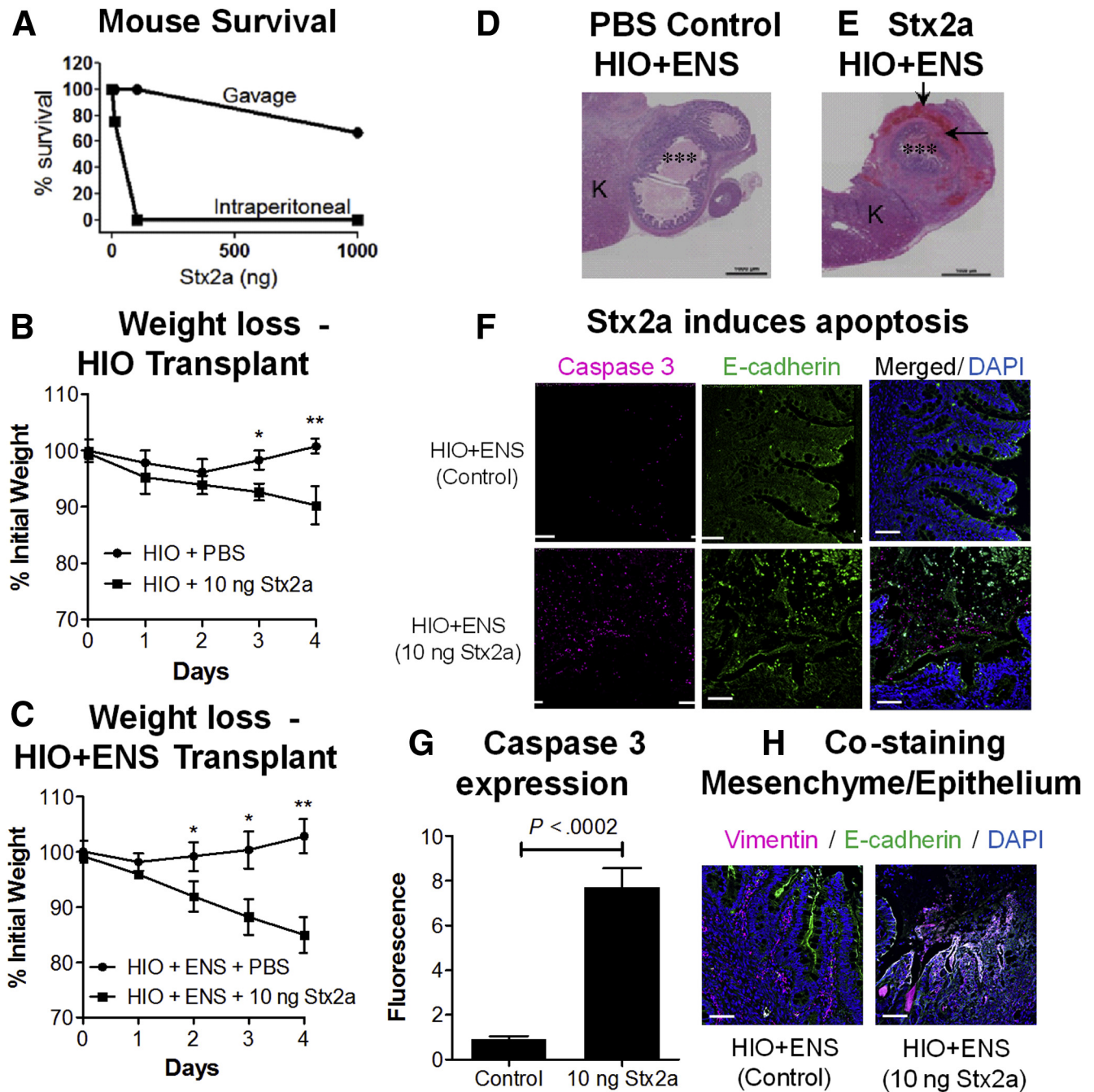


Figure 10. Modeling human responses to Stx in vivo in mice. (A) Susceptibility of mice to Stx2a is dependent on mode of delivery. Mice were challenged with 10, 100, or 1000 ng of Stx2a delivered orally by gavage (3 mice per group) or by IP injection (4 mice per group), and viability was followed up for 5 days. (B and C) Injection of Stx2a into transplanted human organoids causes weight loss in vivo. HIOs transplanted under the kidney capsule of NSG mice were injected with PBS or Stx2a (10 ng). Mice were weighed daily, and the mean percentage of initial weight is plotted \pm SEM, $n = 3$. Statistically significant difference in weight, control vs Stx2a-treated on same day, $*P < .05$, $**P < .01$ by 2-tailed unpaired t test. (B) Stx2a injection into HIO transplants. (C) Stx2a injection into HIO + ENS transplants. (D and E) Stained sections of mouse HIO + ENS transplants. Transplants were injected with PBS or Stx2a, harvested on day 4, and stained with H&E. ***Injected lumen. Black arrows, regions of damage. Representative images of experiments performed in triplicate. (D) PBS-injected HIO + ENS. (E) Stx2a-injected (10 ng) HIO + ENS. (F) Stx2a induces apoptosis in HIO + ENS transplants. Sections of control (top) and Stx2a challenged HIO + ENS (bottom) kidneys stained for apoptotic marker caspase 3 (red), E-cadherin (green), and DNA (4',6-diamidino-2-phenylindole [DAPI], blue). Scale bar: 50 μ m. (G) Quantification of caspase 3. Fluorescence intensity was quantified using ImageJ software, and plotted as means \pm SD, $n = 3$. Statistical significance was assessed using a 2-tailed, unpaired t test. (H) Co-staining for mesenchymal and epithelial markers. Sections of control or Stx2a-challenged HIO + ENS kidneys were stained for vimentin (red) to identify mesenchymal cells, E-cadherin (green) to identify epithelial cells, and DNA (DAPI). Co-staining for E-cadherin and vimentin (yellow) was seen in HIO + ENS challenged with Stx2a. Scale bar: 50 μ m, K, kidney.

Table 2. Summary of Transplanted Mice

Graft injection (mouse ID)	Weight, %	Appearance at death	Cyst	Injection point	Epithelial damage	Blood accumulation in graft
HIO PBS (6471)	101	Ok	1	Not visible	None	Minor: in villi and mesenchyme
HIO PBS (6472)	99	Ok	1.5	Visible	None	Minor: in villi and mesenchyme
HIO PBS (6473)	101	Ok	2	Not visible	None	Minor: in villi and mesenchyme
HIO + ENS PBS (6603)	105	Ok	2	Visible	None	Moderate: in villi and mesenchyme
HIO + ENS PBS (6604)	101	Ok	2	Not visible	None	Minor: in mesenchyme
HIO + ENS PBS (6605)	102	Ok	Uncertain	–	No engraftment	
HIO 10 ng Stx2a (6464)	97	Huddled in corner	1	Not visible	None	Minor: in villi Moderate: in mesenchyme
HIO 10 ng Stx2a (6465)	96	Ok	3	Not visible	None	Minor: in villi and mesenchyme
HIO 10 ng Stx2a (6474)	82	Slow movement	3	Visible	Loss of epithelium in injected cyst	Minor: in villi Moderate: in mesenchyme
HIO + ENS 10 ng Stx2a (6597)	81	Sick, hunched, heavy breathing, lethargic, loss of body hair	1	Not visible	Significant epithelial loss in cyst	Moderate: in villi Significant: in mesenchyme
HIO + ENS 10 ng Stx2a (6598)	88	Ok	1	Not visible	Significant epithelial loss in cyst	Significant: in mesenchyme
HIO + ENS 10 ng Stx2a (6599)	84	Sick, hunched, heavy breathing, lethargic, lost body hair	1	visible	Minor epithelial loss in cyst	Moderate: in villi Minor: in mesenchyme

epithelium and supporting mesenchyme in response to intestinal damage. Necrotic and apoptotic cell death was seen for both mesenchymal and epithelial cells. Wound responses, including changes in transcription and cellular proliferation, also were seen. The presence of both necrotic and apoptotic death could explain results from a study in which inhibition of apoptosis by the proteasome inhibitor bortezomib extended the survival time of mice challenged with Stx2 by approximately a day, but did not prevent death.³⁵ If preventing cellular death is to be an effective intervention, it is likely that both necrosis and apoptosis need to be targeted.

Maintenance of the intestinal epithelial barrier is critical for preventing life-threatening bloodstream infections. The epithelial barrier was remarkably resistant to Stx treatment. HIOs did not lose epithelial barrier function until approximately 48 hours after Stx treatment (Figure 1C and D), and enteroid monolayers maintained epithelial barrier function for 10–15 days (Figures 8A and 9), even though cellular death and loss of polymerized actin was observed. The dramatic differences in time to loss of epithelial barrier function between HIOs (2 days) and the epithelial monolayer (15 days) likely is owing to mesenchymal cells, which are present in the HIOs, but not the enteroids. Purified mesenchymal cells were highly sensitive to Stx. Epithelial cell sensitivity depended on the route of exposure; they were sensitive to luminal exposure, but resistant to Stx added to the medium if mesenchymal cells were absent. Necrox-5, an agent that blocks necrosis, reduced cellular death in both mesenchymal and epithelial cells. It is possible that necrosis of mesenchymal cells releases toxic compounds that cause bystander injury to the epithelial cells.

Alternatively, loss of Wnt production by mesenchymal cells could result in epithelial cell death.³⁶

Epithelial and mesenchymal cells are able to interconvert, and we observed evidence for mesenchymal epithelial transition. The intestinal epithelium is only a single-cell-layer thick. If there is widespread epithelial damage, regeneration from epithelial stem cells in adjacent crypts may be impractical, and mesenchymal cells could be recruited to repair the epithelium. Mesenchymal–epithelial transition has been reported to occur after bacterial infection with *Citrobacter rodentium*.³⁷ Expression of the epithelial marker E-cadherin is the initial step in mesenchymal–epithelial transition.³¹ We observed E-cadherin expression in mesenchymal cells treated with Stx (which inhibits protein synthesis), other toxins including microcystin-LR (which inhibits protein phosphatases), and *C. difficile* toxins (which inactivate small guanosine triphosphatases). Interestingly, LPS did not induce mesenchymal–epithelial transition. Bacterial toxins target key cellular processes and cause pathologic disruption of cellular homeostasis, and mesenchymal–epithelial transition appears to be a general response to epithelial damage. In contrast, the response to LPS is highly scripted. LPS is detected by Toll-like receptors, molecules evolved to recognize pathogens and activate innate immunity. Mesenchymal–epithelial transition does not appear to be wired into this pathway.

Life-threatening HUS results when Stx enters the circulation and accesses susceptible targets in the human vasculature, kidney, and brain. To do this, Stx must escape from the lumen. Transcytosis by enterocytes moves macromolecules from the lumen to the interstitial space, while maintaining the epithelial barrier. Our studies showed that Stx2a

was transported rapidly and efficiently across enteroid monolayers without loss of epithelial barrier function (Figure 8). Recently, the fluid-filled subepithelial interstitium has been shown to be a prelymphatic compartment where fluid drains into the lymph nodes,³⁸ and, ultimately, the bloodstream. Stx transcytosed to the interstitial space would be able access the circulation via this route. Although mice are resistant to Stx2a delivered by the intestinal route, they are highly susceptible to Stx injected IP and rapid weight loss is seen.³⁹ Stx2a injected into HIO transplants in mice lead to significant weight loss as early as day 2 after injection (Figure 10B and C), very similar to what is seen after direct IP injection in mice. Although we were unable to assess maintenance of the epithelial barrier in the transplanted HIOs, transcytosis of Stx to the interstitial space could allow Stx to enter the circulation and access the sensitive tissue targets in the mice. It is important to note that the dose of Stx2a injected into the HIO transplants, which caused weight loss (10 ng), is equivalent to the minimal lethal dose for direct IP injection, suggesting transcytosis is an efficient process.

It is not entirely clear how Stx causes death in mice. Although vascular and kidney involvement is prominent in human disease, in mice lethal disease occurs in the absence of gross pathologic changes to the vasculature or kidney.³⁹ However, lethal doses of Stx in mice are associated with neurologic changes,^{39–41} and these could cause a decrease in feeding and drinking behaviors that result in weight loss. Neurologic complications also are seen in HUS, and are associated with more severe outcomes. In the Germany outbreak in 2011, 48% of the hospitalized patients developed severe neurologic symptoms,⁴² sometimes after the vascular symptoms had resolved.

Currently, there are few treatment options for infection with Stx-producing *E. coli*. Intravenous fluid administered early when diarrhea is present can reduce the risk of renal failure; however, antimicrobial and antidiarrheal agents may increase the risk of developing hemolytic uremic syndrome.⁴³ Mice do not model O157:H7 infection or susceptibility to Shiga toxin. The advent of stem cell-derived human tissue models, both in vitro and in vivo, has a tremendous potential to increase our understanding of Stx disease and lead to development of therapeutic interventions.

Materials and Methods

Culture of HIOs

H1 HIOs obtained from the Pluripotent Stem Cell Facility and the Organoid Core at Cincinnati Children's Hospital and Medical Center were grown as previously described.⁴⁴ H1 HIOs CDH1-mRuby2 (E-cadherin reporter) were obtained from the Wells laboratory.⁴⁵ HIOs typically were used at day 24 of development. Sytox (SYTOX Green Nucleic Acid Stain; cat. S7020, lot 26797W or Orange cat. S11368, lot 1846590; Invitrogen, Thermo Fisher Scientific, Waltham, MA) were used to assess necrosis. Necrox-5 (cat. ALX-430-167; Enzo Life Sciences Inc, Farmingdale, NY) was used to block necrosis.

Toxins and antibodies were obtained from the following sources: Stx2a (cat. NR-4478, lot 62905537; BEI Resources,

Manassas, VA), Stx1 (cat. NR-857, lot 58338341; BEI Resources), TcdA (cat. 152C, lot 15215A5; List Biological Laboratories, Inc, Campbell, CA), TcdB (cat. 155L, lot 15521A2; List Biological Laboratories Inc), microcystin-LR (cat. ALK-350-012-C100, lot L30360; Enzo Life Sciences), LPS (cat. tlr1-3pelps, lot L3P-32-02; InvivoGen, San Diego, CA); monoclonal Stx2, subunit A (cat. NR-845, lot 4469047; BEI Resources), monoclonal Stx2, subunit B (cat. NR-9352, lot 57845852; BEI Resources).

For time course studies Stx2a (30 ng) and Sytox Green were added to the media of day 8 CDH1-mRuby2 spheroids with media changes every 2–3 days.

Preparation of mesenchymal cells. CDH1-mRuby2 HIOs were gently pipetted with large-orifice pipette tips separating the mesenchymal layer, keeping the epithelial layer intact. Free-floating mesenchymal cells were embedded in Matrigel (cat. 354234; Corning, Corning, NY), and incubated in gut medium (advanced Dulbecco's modified Eagle medium/F-12, cat. 12634-010; Life Technologies, Carlsbad, CA), B27 supplement (cat. 12587-010; Life Technologies), N2 supplement (cat. 17502-048; Life Technologies), HEPES buffer (cat. 15630-106; Life Technologies), penicillin and streptomycin (cat. 15140-122; Life Technologies), L-glutamine (cat. 25030-081; Life Technologies), and Recombinant Human Epidermal Growth Factor (cat. 236-EG; R&D Systems, Minneapolis, MN), with changes every 4 days.

Culture of enteroids. Enteroids derived from mouse H1 HIOs transplants were maintained in IntestiCult Organoid Growth Media (OGMH) (cat. 06010; Stemcell Technologies, Cambridge, MA), OGMH component A (cat. 06011; Stemcell), and OGMH component B (cat. 06012; Stemcell) with daily medium changes until they were approximately 1–2 mm. Spheroids were fragmented by passage through a 1-mL insulin syringe, centrifuged at $3800 \times g$ for 1 minute, suspended in Matrigel, and plated in 500 μ L OGMH for 4 days, followed by media changes every 2 days. To induce differentiation, the medium was replaced with differentiation medium (OGMH component A and Dulbecco's modified Eagle medium/F-12 media with 15 mmol/L HEPES in a 1:1 ratio) with daily media changes.

Enteroid monolayers. Enteroid monolayers were prepared using the modified protocol of Zou et al⁴⁶ on 24-well Transwell plates. OGMH component A and component B were mixed in equal volumes containing 10 μ mol/L Y-27632 (cat. 72302; Stemcell), and added to both sides of Transwells coated with collagen type IV from Human Placenta (cat. C5533; Sigma-Aldrich). The medium was replaced by differentiation media on day 2 until the end of the experiment. TEER was measured daily using the ERS-2 volt-ohm meter (Millicell).

Assessment of Stx Toxicity

Stx was diluted in saline and microinjections were performed as previously described.⁴⁴ For epithelial barrier assays, HIOs were injected with saline mixed with 2.5 mg/mL of fluorescent dye, FITC (cat. F-1906, lot 1104-3; Molecular Probes Thermo Fisher Scientific), FITC dextran (cat. FD4; Sigma Aldrich) (average molecular weight, 3000–5000). Sytox was added to the medium at 0.5 μ mol/L for a minimum

of 45 minutes before analysis. For time course experiments, Sytox was allowed to remain in the media continuously.

Mesenchymal cells embedded in Matrigel grown in 500 μ L gut medium were treated with purified Stx2a (30 ng), basolateral medium from Transwells, or other toxins including LPS (10 ng), microcystin-LR (20 ng), *C difficile* toxin TcdA (100 ng), and TcdB (100 ng) for the indicated times. To assess necrosis, isolated mesenchymal cells were incubated for 1 hour with 2 μ mol/L Necrox-5. Fresh gut media containing Stx (30 ng) was added and the cells were incubated for 27 hours.

Stx2a (30 ng) was added to the apical side, or the upper chamber of the Transwell plate. The basolateral media (lower chamber) was collected 24 hours later and toxicity to isolated mesenchymal cells was assessed. To verify the contribution of Stx2a to toxicity, neutralizing antibody against Stx2a subunits A and B was added to the medium.

Immunohistochemistry and Cell Staining

Cryosectioning and immunohistochemical staining (rabbit antivimentin monoclonal antibody, cat. AB92547; Abcam, Cambridge, UK; mouse anti-E-cadherin monoclonal antibody, cat. AB1416; Abcam; rabbit anti-Ki-67 polyclonal antibody, cat. AB5580; Abcam; rabbit anti-active Caspase 3 polyclonal antibody, unconjugated, cat. AB13847; Abcam; rat monoclonal anti-human CD77 antibody (Gb3), cat. YSRMCA579; Accurate Chemical, Westbury, NY; 4',6-diamidino-2-phenylindole, cat. D3571; Invitrogen; Texas Red-X phalloidin (F-actin), cat. T7471, lot 40025A; Molecular Probes; Alexa Fluor-488 goat anti-rabbit IgG (H+L), cat. A11012, lot 1678831; Life Technologies; Alexa Fluor-488 goat anti-mouse IgG (H+L), cat. A11001, lot 1726530; Life Technologies; Alexa Fluor-594 goat anti-mouse IgG (H+L), cat. A11005, lot 1890858; Life Technologies; Alexa Fluor-594 goat anti-rat IgG IgM (μ chain), cat. A21213, lot 1458639; Life Technologies; goat serum, cat. S-1000; Vector Laboratories, Burlingame, CA) was performed as previously described.⁴⁴ For whole-mount staining, organoids were permeabilized with 0.5% Triton X-100 (Sigma-Aldrich, St. Louis, MO) during initial blocking for 3 hours at room temperature.

Microscopy

For cryosectioned organoids and whole-mount enteroids, images were obtained on a Zeiss LSM710 Live Duo Confocal Microscope (Oberkochen, Germany). For live imaging in time course studies, CDH1-mRuby2 HIOs were placed on the Ibidi gas incubation system (cat. 11922; Fitchburg, WI) and imaged on the Zeiss LSM510 NLO Two-Photon Microscope. Isolated mesenchymal cells were observed under the Zeiss LSM510 NLO Two-Photon Microscope. For FITC-injected intact organoids, fluorescent images were obtained using a stereomicroscope (Eclipse TE2000-U; Nikon, Tokyo, Japan). Fluorescent signal was quantified using ImageJ software (National Institutes of Health, Bethesda, MD).

Bioinformatics RNA sequencing data analysis. RNA sequencing was performed by the University of Cincinnati Genomics, Epigenomics and Sequencing Core.⁴⁴ Results are

deposited in GEO (GEO submission: GSE144633; geo@ncbi.nlm.nih.gov). Three independent HIOs were used for each experimental condition. Sequence reads were performed using the TopHat aligner,⁴⁷ reads for known transcripts were counted using Bioconductor packages,⁴⁸ and differential expression analysis was performed for each using the edgeR package.⁴⁹ Statistical significance of differential expression, indicated in the padj columns in [Supplementary Tables 1 and 2](#), is based on the false-discovery rate-adjusted *P* values.⁵⁰ Gene ontology analysis was performed with GOrilla.⁵¹

In vivo studies. To assess susceptibility of the NSG line to Stx, NSG mice (cat. 005557; Jackson Laboratory, Bar Harbor, ME) were challenged with 10, 100, or 1000 ng of Stx2a delivered orally by gavage (3 mice per group) or by IP injection (4 mice per group), and viability was followed up for 4 days. To assess human intestinal susceptibility to Stx in vivo, HIO and HIO + ENS were transplanted under the kidney capsule of NSG mice and allowed to grow for 6 weeks as previously described.^{22,23} Transplants were accessed surgically and the lumen was injected with 20 μ L PBS or PBS with 1 or 10 ng Stx2a. Incisions were closed. The mice were weighed daily and killed on day 4. The kidneys were harvested, fixed, and sectioned for histology. Protocol IACUC2018-0092 was approved by the CCHMC Institutional Animal Care and Use Committee.

Quantification and statistical analysis. Statistical analyses were performed using GraphPad Prism 5. Specific tests are indicated in the figure legend.

All authors had access to the study data and have reviewed and approved the final manuscript.

References

1. Majowicz SE, Scallan E, Jones-Bitton A, Sargeant JM, Stapleton J, Angulo FJ, Yeung DH, Kirk MD. Global incidence of human Shiga toxin-producing *Escherichia coli* infections and deaths: a systematic review and knowledge synthesis. *Foodborne Pathog Dis* 2014; 11:447–455.
2. Tarr PI, Gordon CA, Chandler WL. Shiga-toxin-producing *Escherichia coli* and haemolytic uraemic syndrome. *Lancet* 2005;365:1073–1086.
3. Jacobson JM, Yin J, Kitov PI, Mulvey G, Griener TP, James MNG, Armstrong G, Bundle DR. The crystal structure of Shiga toxin type 2 with bound disaccharide guides the design of a heterobifunctional toxin inhibitor. *J Biol Chem* 2014;289:885–894.
4. Pellino CA, Karve SS, Pradhan S, Weiss AA. AB5 pre-assembly is not required for Shiga toxin activity. *J Bacteriol* 2016;198:1621–1630.
5. Endo Y, Tsurugi K, Yutsudo T, Takeda Y, Ogasawara T, Igarashi K. Site of action of a Vero toxin (VT2) from *Escherichia coli* O157:H7 and of Shiga toxin on eukaryotic ribosomes. RNA N-glycosidase activity of the toxins. *Eur J Biochem FEBS* 1988;171:45–50.
6. Obata F, Tohyama K, Bonev AD, Kolling GL, Keepers TR, Gross LK, Nelson MT, Sato S, Obrigg TG. Shiga toxin 2 affects the central nervous system through receptor globotriaosylceramide localized to neurons. *J Infect Dis* 2008;198:1398–1406.

7. Ling H, Boodhoo A, Hazes B, Cummings MD, Armstrong GD, Brunton JL, Read RJ. Structure of the Shiga-like toxin I B-pentamer complexed with an analogue of its receptor Gb3. *Biochemistry* 1998; 37:1777–1788.
8. Lingwood C. Role of verotoxin receptors in pathogenesis. *Trends Microbiol* 1996;4:147–153.
9. Waddell T, Head S, Petric M, Cohen A, Lingwood C. Globotriosyl ceramide is specifically recognized by the *Escherichia coli* verocytotoxin 2. *Biochem Biophys Res Commun* 1988;152:674–679.
10. Okuda T, Tokuda N, Numata S, Ito M, Ohta M, Kawamura K, Wiels J, Urano T, Tajima O, Furukawa K, Furukawa K. Targeted disruption of Gb3/CD77 synthase gene resulted in the complete deletion of globo-series glycosphingolipids and loss of sensitivity to verotoxins. *J Biol Chem* 2006;281:10230–10235.
11. Kvalvaag AS, Pust S, Sundet KI, Engedal N, Simm R, Sandvig K. The ERM proteins ezrin and moesin regulate retrograde Shiga toxin transport: the ERM proteins regulate retrograde transport. *Traffic* 2013;14:839–852.
12. Parello C, Mayer C, Lee B, Motomochi A, Kurosawa S, Stearns-Kurosawa D. Shiga toxin 2-induced endoplasmic reticulum stress is minimized by activated protein C but does not correlate with lethal kidney injury. *Toxins* 2015;7:170–186.
13. Cherla RP, Lee S-Y, Tesh VL. Shiga toxins and apoptosis. *FEMS Microbiol Lett* 2003;228:159–166.
14. Marquez LB, Velazquez N, Repetto HA, Paton AW, Paton JC, Ibarra C, Silberstein C. Effects of *Escherichia coli* subtilase cytotoxin and Shiga toxin 2 on primary cultures of human renal tubular epithelial cells. *PLoS One* 2014;9:e87022.
15. Kaeffer B. Survival of exfoliated epithelial cells: a delicate balance between anoikis and apoptosis. *J Biomed Biotechnol* 2011;2011:1–9.
16. Negroni A, Cucchiara S, Stronati L. Apoptosis, necrosis, and necroptosis in the gut and intestinal homeostasis. *Mediators Inflamm* 2015;2015:1–10.
17. Petruzzello-Pellegrini TN, Yuen DA, Page AV, Patel S, Soltyk AM, Matouk CC, Wong DK, Turgeon PJ, Fish JE, Ho JJD, Steer BM, Khajooee V, Tigdi J, Lee WL, Motto DG, Advani A, Gilbert RE, Karumanchi SA, Robinson LA, Tarr PI, Liles WC, Brunton JL, Marsden PA. The CXCR4/CXCR7/SDF-1 pathway contributes to the pathogenesis of Shiga toxin-associated hemolytic uremic syndrome in humans and mice. *J Clin Invest* 2012; 122:759–776.
18. Russo LM, Melton-Celsa AR, Smith MA, Smith MJ, O'Brien AD. Oral intoxication of mice with Shiga toxin type 2a (Stx2a) and protection by anti-Stx2a monoclonal antibody 11E10. *Infect Immun* 2014;82:1213–1221.
19. Spence JR, Mayhew CN, Rankin SA, Kuhar MF, Vallance JE, Tolle K, Hoskins EE, Kalinichenko VV, Wells SI, Zorn AM, Shroyer NF, Wells JM. Directed differentiation of human pluripotent stem cells into intestinal tissue in vitro. *Nature* 2011;470:105–109.
20. McCracken KW, Howell JC, Wells JM, Spence JR. Generating human intestinal tissue from pluripotent stem cells in vitro. *Nat Protoc* 2011;6:1920–1928.
21. Chong Y, Fitzhenry R, Heuschkel R, Torrente F, Frankel G, Phillips AD. Human intestinal tissue tropism in *Escherichia coli* O157:H7-initial colonization of terminal ileum and Peyer's patches and minimal colonic adhesion ex vivo. *Microbiology* 2007;153:794–802.
22. Watson CL, Mahe MM, Múnera J, Howell JC, Sundaram N, Poling HM, Schweitzer JI, Vallance JE, Mayhew CN, Sun Y, Grabowski G, Finkbeiner SR, Spence JR, Shroyer NF, Wells JM, Helmrath MA. An in vivo model of human small intestine using pluripotent stem cells. *Nat Med* 2014;20:1310–1314.
23. Workman MJ, Mahe MM, Trisno S, Poling HM, Watson CL, Sundaram N, Chang C-F, Schiesser J, Aubert P, Stanley EG, Elefanti AG, Miyaoka Y, Mandegar MA, Conklin BR, Neunlist M, Brugmann SA, Helmrath MA, Wells JM. Engineered human pluripotent-stem-cell-derived intestinal tissues with a functional enteric nervous system. *Nat Med* 2016;23:49–59.
24. Scheutz F, Teel LD, Beutin L, Pierard D, Buvens G, Karch H, Mellmann A, Caprioli A, Tozzoli R, Morabito S, Strockbine NA, Melton-Celsa AR, Sanchez M, Persson S, O'Brien AD. Multicenter evaluation of a sequence-based protocol for subtyping Shiga toxins and standardizing Stx nomenclature. *J Clin Microbiol* 2012; 50:2951–2963.
25. Tesh VL, Burris JA, Owens JW, Gordon VM, Wadolkowski EA, O'Brien AD, Samuel JE. Comparison of the relative toxicities of Shiga-like toxins type I and type II for mice. *Infect Immun* 1993;61:3392–3402.
26. Fuller CA, Pellino CA, Flagler MJ, Strasser JE, Weiss AA. Shiga toxin subtypes display dramatic differences in potency. *Infect Immun* 2011;79:1329–1337.
27. Boerlin P, McEwen SA, Boerlin-Petzold F, Wilson JB, Johnson RP, Gyles CL. Associations between virulence factors of Shiga toxin-producing *Escherichia coli* and disease in humans. *J Clin Microbiol* 1999;37:497–503.
28. Kawano K, Okada M, Haga T, Maeda K, Goto Y. Relationship between pathogenicity for humans and stx genotype in Shiga toxin-producing *Escherichia coli* serotype O157. *Eur J Clin Microbiol Infect Dis* 2007; 27:227–232.
29. MacDonald IA, Gould IM, Curnow J. Epidemiology of infection due to *Escherichia coli* O157: a 3-year prospective study. *Epidemiol Infect* 1996;116:279–284.
30. Slutsker L, Ries AA, Greene KD, Wells JG, Hutwagner L, Griffin PM. *Escherichia coli* O157:H7 diarrhea in the United States: clinical and epidemiologic features. *Ann Intern Med* 1997;126:505–513.
31. Alotaibi H, Basilicata MF, Shehwana H, Kosowan T, Schreck I, Braeutigam C, Konu O, Brabletz T, Stemmler MP. Enhancer cooperativity as a novel mechanism underlying the transcriptional regulation of E-cadherin during mesenchymal to epithelial transition. *Biochim Biophys Acta* 2015;1849:731–742.
32. Hurley BP, Jacewicz M, Thorpe CM, Lincicome LL, King AJ, Keusch GT, Acheson DWK. Shiga toxins 1 and 2 translocate differently across polarized intestinal epithelial cells. *Infect Immun* 1999;67:6670–6677.
33. Zumbun SD, Hanson L, Sinclair JF, Freedy J, Melton-Celsa AR, Rodriguez-Canales J, Hanson JC, O'Brien AD.

- Human intestinal tissue and cultured colonic cells contain globotriaosylceramide synthase mRNA and the alternate Shiga toxin receptor globotetraosylceramide. *Infect Immun* 2010;78:4488–4499.
34. Schüller S, Frankel G, Phillips AD. Interaction of Shiga toxin from *Escherichia coli* with human intestinal epithelial cell lines and explants: Stx2 induces epithelial damage in organ culture. *Cell Microbiol* 2004;6:289–301.
 35. Hattori T, Watanabe-Takahashi M, Ohoka N, Hamabata T, Furukawa K, Nishikawa K, Naito M. Proteasome inhibitors prevent cell death and prolong survival of mice challenged by Shiga toxin. *FEBS Open Bio* 2015;5:605–614.
 36. Valenta T, Degirmenci B, Moor AE, Herr P, Zimmerli D, Moor MB, Hausmann G, Cantù C, Aguet M, Basler K. Wnt ligands secreted by subepithelial mesenchymal cells are essential for the survival of intestinal stem cells and gut homeostasis. *Cell Rep* 2016;15:911–918.
 37. Chandrakesan P, Roy B, Jakkula LUMR, Ahmed I, Ramamoorthy P, Tawfik O, Papineni R, Houchen C, Anant S, Umar S. Utility of a bacterial infection model to study epithelial–mesenchymal transition, mesenchymal–epithelial transition or tumorigenesis. *Oncogene* 2014;33:2639–2654.
 38. Benias PC, Wells RG, Sackey-Aboagye B, Klavan H, Reidy J, Buonocore D, Miranda M, Kornacki S, Wayne M, Carr-Locke DL, Theise ND. Structure and distribution of an unrecognized interstitium in human tissues. *Sci Rep* 2018;8:4947.
 39. Pradhan S, Pellino C, MacMaster K, Coyle D, Weiss AA. Shiga toxin mediated neurologic changes in murine model of disease. *Front Cell Infect Microbiol* 2016;6:114.
 40. Pinto A, Cangelosi A, Geoghegan PA, Goldstein J. Dexamethasone prevents motor deficits and neurovascular damage produced by Shiga toxin 2 and lipopolysaccharide in the mouse striatum. *Neuroscience* 2017;344:25–38.
 41. Berdasco C, Pinto A, Calabró V, Arenas D, Cangelosi A, Geoghegan P, Evelson P, Goldstein J. Shiga toxin 2 from enterohemorrhagic *Escherichia coli* induces reactive glial cells and neurovascular disarrangements including edema and lipid peroxidation in the murine brain hippocampus. *J Biomed Sci* 2019;26:16.
 42. Magnus T, Rother J, Simova O, Meier-Cillien M, Repenthin J, Moller F, Gbadamosi J, Panzer U, Wengenroth M, Hagel C, Kluge S, Stahl RK, Wegscheider K, Urban P, Eckert B, Glatzel M, Fiehler J, Gerloff C. The neurological syndrome in adults during the 2011 northern German *E. coli* serotype O104:H4 outbreak. *Brain* 2012;135:1850–1859.
 43. Shane AL, Mody RK, Crump JA, Tarr PI, Steiner TS, Kotloff K, Langley JM, Wanke C, Warren CA, Cheng AC, Cantey J, Pickering LK. 2017 Infectious Diseases Society of America clinical practice guidelines for the diagnosis and management of infectious diarrhea. *Clin Infect Dis* 2017;65:e45–e80.
 44. Karve SS, Pradhan S, Ward DV, Weiss AA. Intestinal organoids model human responses to infection by commensal and Shiga toxin producing *Escherichia coli*. *PLoS One* 2017;12:e0178966.
 45. Ouchi R, Togo S, Kimura M, Shinozawa T, Koido M, Koike H, Thompson W, Karns RA, Mayhew CN, McGrath PS, McCauley HA, Zhang R-R, Lewis K, Hakozaki S, Ferguson A, Saiki N, Yoneyama Y, Takeuchi I, Mabuchi Y, Akazawa C, Yoshikawa HY, Wells JM, Takebe T. Modeling steatohepatitis in humans with pluripotent stem cell-derived organoids. *Cell Metab* 2019;30:374–384.e6.
 46. Zou WY, Blutt SE, Crawford SE, Ettayebi K, Zeng X-L, Saxena K, Ramani S, Karandikar UC, Zachos NC, Estes MK. Human intestinal enteroids: new models to study gastrointestinal virus infections. In: Turksen K, ed. *Organoids*. New York: Springer, 2017:229–247.
 47. Trapnell C, Pachter L, Salzberg SL. TopHat: discovering splice junctions with RNA-Seq. *Bioinformatics* 2009;25:1105–1111.
 48. Huber W, Carey VJ, Gentleman R, Anders S, Carlson M, Carvalho BS, Bravo HC, Davis S, Gatto L, Girke T, Gottardo R, Hahne F, Hansen KD, Irizarry RA, Lawrence M, Love MI, MacDonald J, Obenchain V, Oleś AK, Pagès H, Reyes A, Shannon P, Smyth GK, Tenenbaum D, Waldron L, Morgan M. Orchestrating high-throughput genomic analysis with Bioconductor. *Nat Methods* 2015;12:115–121.
 49. Anders S, McCarthy DJ, Chen Y, Okoniewski M, Smyth GK, Huber W, Robinson MD. Count-based differential expression analysis of RNA sequencing data using R and Bioconductor. *Nat Protoc* 2013;8:1765–1786.
 50. Storey JD, Tibshirani R. Statistical significance for genomewide studies. *Proc Natl Acad Sci* 2003;100:9440–9445.
 51. Eden E, Navon R, Steinfeld I, Lipson D, Yakhini Z. GOrrilla: a tool for discovery and visualization of enriched GO terms in ranked gene lists. *BMC Bioinformatics* 2009;10:48.

Received December 10, 2019. Accepted February 26, 2020.

Correspondence

Address correspondence to: Alison Weiss, PhD, Molecular Genetics, Biochemistry, and Microbiology, Medical Sciences Building, Room 2254, 231 Albert Sabin Way, ML 524, University of Cincinnati, Cincinnati, Ohio 45267-0524. e-mail: alison.weiss@uc.edu; fax: (513) 558-8474.

Author contributions

Suman Pradhan was responsible for the study concept and design, acquisition of data, analysis and interpretation of data, drafting of the manuscript, critical revision of the manuscript for important intellectual content, and statistical analysis; Sayali S. Karve was responsible for the study concept and design, acquisition of data, analysis and interpretation of data, drafting of the manuscript, critical revision of the manuscript for important intellectual content, and statistical analysis; Alison A. Weiss was responsible for the study concept and design, data analysis and interpretation of data, drafting of the manuscript, critical revision of the manuscript for important intellectual content, statistical analysis, obtained funding, and study supervision; Jennifer Hawkins was responsible for the study concept and design, acquisition of data, analysis and interpretation of data, technical or material support, and study supervision; Nambirajan Sundaram was responsible for the acquisition of data and technical or material support; Holly M. Poling was responsible for the acquisition of data, analysis and interpretation of data, and technical or material support; Michael A. Helmrath was responsible for the study concept and design, acquisition of data, analysis and interpretation of data, obtained funding, and study supervision; James M. Wells was responsible for the study concept and design, analysis and interpretation of data, critical revision of the manuscript for important intellectual content, and technical or material support; and Heather A. McCauley was responsible for

the critical revision of the manuscript for important intellectual content and technical or material support.

Conflicts of interest

The authors disclose no conflicts.

Funding

This work was supported by National Institutes of Health grants R01-AI064893, U19-AI116491, R21AI115003, and R01AI139027; the Center for Clinical and Translational Science and Training, Advancing Translational Sciences Award Number 1UL1TR001425-01; and by National Institute of Diabetes and Digestive and Kidney Diseases grant P30 DK078392

(Pluripotent Stem Cell and Organoid Core and Live Microscopy Core) of the Digestive Disease Research Core Center in Cincinnati. The Biodefense and Emerging Infections Research Resources Repository provided purified Stx2a, Stx1, and antibodies to Stx2. Supported by the National Institute of Diabetes and Digestive and Kidney Diseases and National Institute of Allergy and Infectious Diseases grant U01DK103117 (M.A.H.), and generous philanthropic support also was received from the Farmer Family Foundation. Also supported by American Diabetes Association Postdoctoral Fellowship 1-17-PDF-102 (H.A.M.).

The study sponsors had no role in the study design, collection, analysis, or interpretation of data.